

# The Earth Observing System Microwave Limb Sounder (EOS MLS) on the Aura Satellite

Joe W. Waters, Lucien Froidevaux, Robert S. Harwood, Robert F. Jarnot, Herbert M. Pickett, William G. Read, Peter H. Siegel, Richard E. Cofield, Mark J. Filipiak, Dennis A. Flower, James R. Holden, Gary K. Lau, Nathaniel J. Livesey, Gloria L. Manney, Hugh C. Pumphrey, Michelle L. Santee, Dong L. Wu, David T. Cuddy, Richard R. Lay, Mario S. Loo, Vincent S. Perun, Michael J. Schwartz, Paul C. Stek, Robert P. Thurstans, Mark A. Boyles, Kumar M. Chandra, Marco C. Chavez, Gun-Shing Chen, Bharat V. Chudasama, Randy Dodge, Ryan A. Fuller, Michael A. Girard, Jonathan H. Jiang, Yibo Jiang, Brian W. Knosp, Remi C. LaBelle, Jonathan C. Lam, Karen A. Lee, Dominick Miller, John E. Oswald, Navnit C. Patel, David M. Pukala, Ofelia Quintero, David M. Scaff, W. Van Snyder, Michael C. Tope, Paul A. Wagner, and Marc J. Walch

**Abstract**—EOS MLS measures several atmospheric chemical species (OH, HO<sub>2</sub>, H<sub>2</sub>O, O<sub>3</sub>, HCl, ClO, HOCl, BrO, HNO<sub>3</sub>, N<sub>2</sub>O, CO, HCN, CH<sub>3</sub>CN, volcanic SO<sub>2</sub>), cloud ice, temperature and geopotential height to improve our understanding of stratospheric ozone chemistry, the interaction of composition and climate, and pollution in the upper troposphere. All measurements are made simultaneously and continuously, during both day and night. The instrument uses heterodyne radiometers that observe thermal emission from the atmospheric limb in broad spectral regions centered near 118, 190, 240 and 640 GHz, and 2.5 THz. It was launched 15 July 2004 on the NASA Aura satellite and started full-up science operations on 13 August 2004. An atmospheric limb scan and radiometric calibration for all bands are performed routinely every 25 seconds. Vertical profiles are retrieved every 165 km along the suborbital track, covering 82° S to 82° N latitudes on each orbit. Instrument performance to date has been excellent, data have been made publicly available, and initial science results have been obtained.

**Index Terms** — remote sensing, microwave, submillimeter wave, stratosphere

## I. INTRODUCTION

EOS MLS, on the NASA Aura satellite launched 15 July 2004, uses the microwave limb sounding technique [1] to provide information on Earth's upper troposphere, stratosphere and mesosphere. It is an advanced follow-on to the first MLS [2][3] on the Upper Atmosphere Research Satellite (UARS) launched 12 September 1991. The major objective of UARS MLS was, in response to the industrial chlorofluorocarbon threat to the ozone layer [4], to provide global information on chlorine monoxide (ClO) – the dominant form of chlorine that destroys ozone. The UARS MLS design was ‘frozen’ before discovery of the Antarctic ozone

hole [5][6], and the design was for the middle and upper stratospheric measurements thought most important at the time. It was, however, able to provide valuable information for assessing the chlorine destruction of lower stratospheric ozone in the Antarctic and Arctic winters [7][8]. UARS MLS also provided additional measurements beyond stratospheric ClO, O<sub>3</sub> and H<sub>2</sub>O for which it was designed, most notable of which are upper tropospheric H<sub>2</sub>O vapor [9]-[11] and cloud ice [12], stratospheric HNO<sub>3</sub> [13][14], and temperature variances associated with atmospheric gravity waves [15][16]. A summary of scientific highlights from UARS MLS through 1999 is in [3]. The MLS web site (<http://mls.jpl.nasa.gov>) contains an updated list of MLS-related scientific publications.

EOS MLS is greatly improved over UARS MLS in having (1) many more stratospheric measurements for chemical composition and dynamical tracers, (2) more and better upper tropospheric measurements, and (3) better global and temporal coverage and resolution. These improvements were possible because of (1) advances in technology that have extended the spectral range and bandwidth of microwave heterodyne radiometer systems that can be operated on a satellite, (2) design of EOS MLS for upper tropospheric and lower stratospheric measurements, (3) the Aura polar orbit that allows nearly pole-to-pole coverage on each orbit and measurements made in the orbit plane than enables more accurate handling of atmospheric gradients in the line-of-sight direction. The EOS MLS atmospheric measurement objectives are shown in Fig. 1.

An overview of the Aura mission is in [17]. Companion instruments to MLS on Aura are the Tropospheric Emission Spectrometer TES [18], the Ozone Monitoring Instrument OMI [19], and the High Resolution Dynamics Limb Sounder HIRDLS [17].

## II. MEASUREMENT TECHNIQUE

Microwave limb sounding remotely measures atmospheric parameters by observing millimeter- and submillimeter-wavelength thermal emission as the instrument field-of-view (FOV) is scanned through the atmospheric limb from above. Features of the technique, described further in [1], include:

Manuscript received May 1, 2005; revised 3 October, 2005. Work at the Jet Propulsion Laboratory, California Institute of Technology, was done under contract with the U.S. National Aeronautics and Space Administration. Work at The University of Edinburgh was done with support from the U.K. Natural Environment Research Council.

J. W. Waters is with the Jet Propulsion Laboratory, Pasadena, CA 91109 USA (818-354-3025; fax 818-393-5065, e-mail: [joe@mls.jpl.nasa.gov](mailto:joe@mls.jpl.nasa.gov)). All other authors are also with JPL, except for R. S. Harwood, M. J. Filipiak and H. C. Pumphrey who are with The University of Edinburgh, Edinburgh, Scotland, EH9 3JZ.

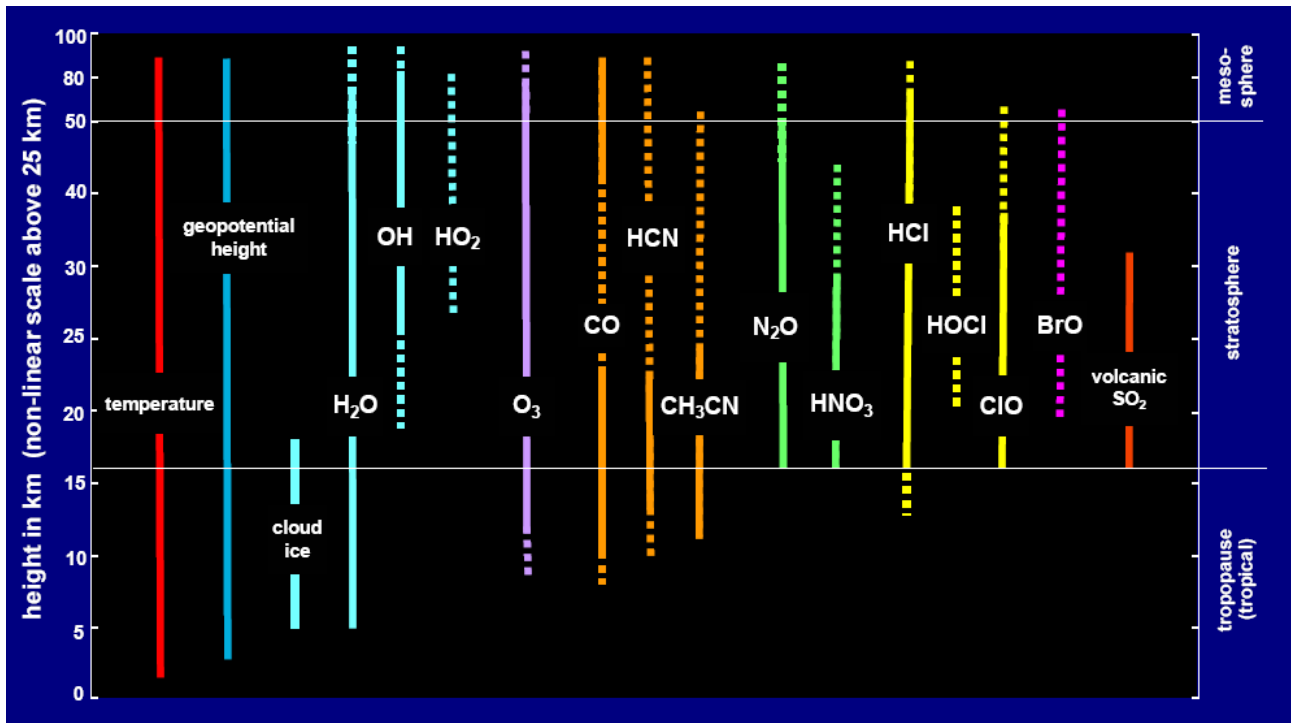


Fig. 1. EOS MLS scientific measurement objectives. Solid lines indicate generally useful precision for individual profiles. Dotted lines indicate that zonal (or other) averages are generally needed to obtain useful precision. Solid lines for lower stratospheric and upper tropospheric HCN and CH<sub>3</sub>CN apply to enhanced abundances expected from biomass burning injections. The height ranges shown here indicate what is ultimately expected to be achieved, and not necessarily achieved with initial data processing. Different colors indicate different chemical families.

- 1) the ability to measure many atmospheric gases, with emission from molecular oxygen (and other molecules) providing temperature and pressure;
- 2) reliable measurements, even in the presence of aerosol, cirrus, or polar stratospheric clouds that can degrade or prevent shorter-wavelength ultraviolet, visible and infrared techniques (Fig. 3 of [3] shows the small effect of dense volcanic aerosol on MLS measurements.);
- 3) the ability to measure cloud ice and obtain information on ice particle size for dense ice clouds that saturate or block shorter-wavelength techniques;
- 4) the ability to make measurements at all times of day and night, and thus provide global coverage on a daily basis;
- 5) the ability to spectrally resolve emission lines at all altitudes, which allows measurements of very weak lines in the presence of nearby strong ones.

The widths of atmospheric spectral lines in the millimeter and submillimeter-wavelength spectral regions used by MLS are dominated by pressure (collisional) broadening throughout the troposphere and stratosphere, resulting in the linewidth being a nearly exponentially-decreasing function of height up to ~50-70 km. Doppler broadening, which is proportional to the line frequency and only weakly-dependent on height (through temperature), dominates at higher altitudes. Fig. 2 shows linewidth variation with height for representative spectral lines measured by EOS MLS.

The instrumentation used for MLS measurements has stable and accurate calibration. Fig. 3 shows data indicating the long-term stability of the UARS MLS antenna system reflectivity.

‘Space radiances,’ the radiances measured through the antenna system when it is pointed well above the atmosphere and calibrated in the same manner as the atmospheric radiances [20] are plotted, after subtraction of an initial radiance offset of a few kelvins. The absolute mirror reflectivities in all spectral bands were inferred from reflectivity measurements using a silver plate standard; the inferred reflectivity for the primary mirror was  $0.9956 \pm 0.0008$  for bands covering 202-204 GHz (and the image sideband at 200-201 GHz) [20] (inferred reflectivity values for the EOS MLS primary mirror vary from 0.9977 at 118 GHz to 0.9889 at 640 GHz [21]). The typical in-orbit temperature of the antenna is ~250 K, and the trend in the observed space radiances thus corresponds to an upper limit of  $\sim 3 \times 10^{-5}$  (= 0.007 K / 250 K) change per year in the overall

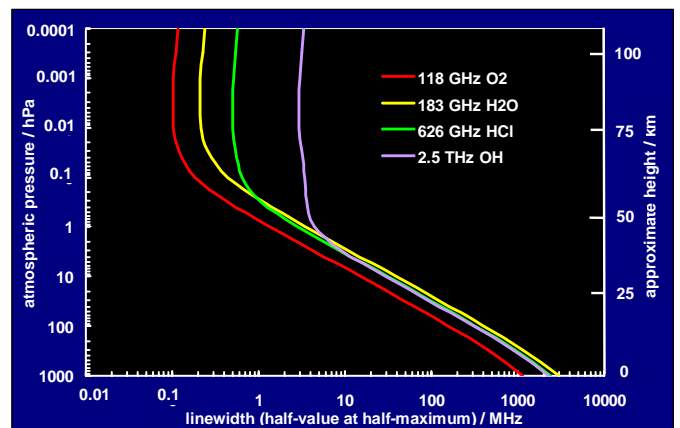


Fig. 2. Linewidth versus height for some spectral lines measured by EOS MLS.

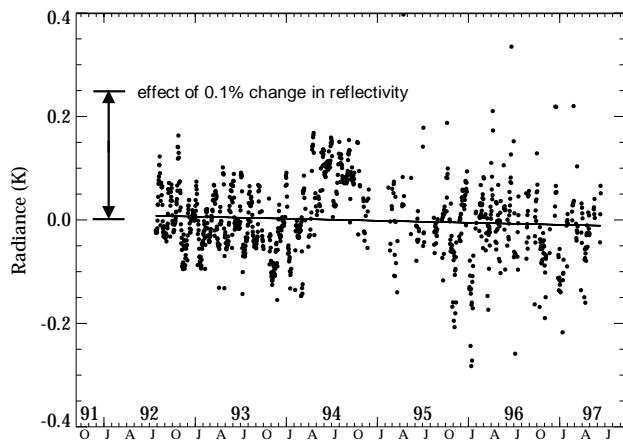


Fig. 3. Time-series of 205 GHz UARS MLS space radiances. The marker on the left shows the effect that 0.1% change in reflectivity, with concomitant emissivity change, would have. The nearly horizontal line is a best fit to the radiance trend over the  $\sim 5$  year period analyzed, and has slope of  $-0.004$  K/year with  $\pm 0.003$  K/year  $2\sigma$  uncertainty.

antenna system reflectivity, or an upper limit of  $\sim 0.015\%$  in the change over the 5-year period analyzed. Scatter in the plotted points is thought due, mainly, to limitations of the simple thermal model that was used to subtract the small amount of emission from the antenna. Degradation in reflectivity of the antenna reflector surfaces is thought to dominate any degradation in instrument radiometric calibration because these are the only surfaces in the signal path that are exposed to the degrading effects of solar ultraviolet radiation and atomic oxygen. Antenna reflectivity affects overall radiometric calibration errors proportionally, and these data therefore imply an upper limit of  $\sim 3 \times 10^{-5}$  per year degradation in UARS MLS radiometric calibration due to this effect. Similar performance is expected from EOS MLS. Uncertainty in instrument absolute calibration accuracy [20]-[23] and in the spectroscopic parameters (e.g., [24]-[27]) used in data processing can be as small as a few percent.

### III. SCIENTIFIC OBJECTIVES

The overall scientific objectives of EOS MLS are to:

- 1) determine if stratospheric ozone chemistry is recovering,
- 2) quantify aspects of how composition affects climate, and
- 3) study aspects of pollution in the upper troposphere.

#### A. Stratospheric ozone chemistry

An overarching question is whether global stratospheric ozone will recover as expected in the next several decades, following the international regulations on ozone depleting substances. Stratospheric total chlorine will be near its peak during the Aura mission, and stratospheric total bromine may still be increasing, although more slowly than previously [28]. Climate change could possibly delay ozone recovery through stratospheric cooling that can exacerbate some ozone chemical destruction processes, and possibly through changes in transport across the tropical tropopause that could alter the amount

of  $\text{H}_2\text{O}$  (and perhaps other substances) in the stratosphere, affecting ozone chemistry and recovery.

EOS MLS produces an extensive dataset for tracking stratospheric ozone chemistry. It provides the first global measurements of OH and  $\text{HO}_2$ , the chemically-reactive species in hydrogen chemistry that dominates ozone destruction at  $\sim 20$ - $25$  km outside winter polar regions, and at heights above  $\sim 45$  km. Our present understanding of hydrogen chemistry in the upper stratosphere is in question due to some observations of OH that are in disagreement with current theory [29]. One MLS objective is to resolve this discrepancy.

Also, for the first time globally, EOS MLS simultaneously measures stratospheric chlorine in both its dominant ‘reservoir’ form (HCl) that is not directly involved in ozone destruction and is a measure of total chlorine in the stratosphere, and the dominant ‘radical’ form (ClO) that is responsible for ozone destruction. These two measurements allow tracking of both total chlorine in the stratosphere, and the form of stratospheric chlorine that destroys ozone; having them simultaneously provides a stringent test of our understanding of stratospheric chlorine chemistry and its possible changes. MLS measures BrO, which is both the dominant form of bromine in the stratosphere as well as the form that destroys ozone. The MLS simultaneous measurements of ClO, HCl,  $\text{HNO}_3$ ,  $\text{N}_2\text{O}$ ,  $\text{H}_2\text{O}$ ,  $\text{O}_3$  and temperature are important for tracking the processes affecting ozone destruction in the polar winter lower stratosphere (e.g., [7][8][13]). The Arctic, in particular, may be at a threshold for more severe ozone loss due to climate change while stratospheric chlorine loading is still high.

Quantifying processes in the tropical tropopause region, where air enters the stratosphere, is important for assessing changes in ozone chemistry and recovery. Our current knowledge of these processes is so poor, however, that we cannot even explain the sign of the observed trend in stratospheric  $\text{H}_2\text{O}$ . How and why stratospheric humidity has been increasing for the last few decades [30] has important implications for stratospheric  $\text{O}_3$  [31]. The simultaneous and continuous MLS measurements of  $\text{H}_2\text{O}$ , cloud ice and temperature over several years will help answer this question.

#### B. Composition effects on climate variability

A key uncertainty in predicting future climate changes is the response of tropospheric  $\text{H}_2\text{O}$  to changes in other greenhouse gas concentrations. Depending upon details of the process affecting it, upper tropospheric  $\text{H}_2\text{O}$  can either amplify or attenuate the effects of changes in other greenhouse gases. Understanding the mechanisms that control humidity of the tropical upper troposphere is essential for determining the nature of the  $\text{H}_2\text{O}$  feedback on climate, and thus for improving climate change predictions. The small amounts of  $\text{H}_2\text{O}$  in the upper troposphere have a particularly strong infrared radiative effect, due to the low temperatures there, and exert enormous leverage on Earth’s radiative balance. Of particular importance is the moisture in the dry subtropical regions, which has a large cooling effect on the whole tropics [32].

Measurement of upper tropospheric humidity (UTH) on a global scale from satellite has historically been difficult, due to its relatively small abundance and the presence of clouds. This has limited the progress in understanding processes that control

UTH and its effect on climate variability. The MLS technique, with its combined sensitivity and ability to measure in the presence of ice clouds, can produce good daily global measurements of UTH as demonstrated from UARS [9]-[11]. EOS MLS gives better UTH and cloud ice measurements than UARS MLS; these, along with the MLS simultaneous measurements of temperature, will help improve our understanding of climate variability. The MLS measurements of cloud ice water content will provide data on the supply of water to the upper troposphere – helping, for example, to determine what fraction of water in convective air parcels remains in condensed form that can fall out. Variation in the observed UTH over seasonal to interannual time scales will provide insight into how different forcings, such as El Niño, may affect climate variability. MLS measurements of the tracer CO provide information on the origin of air masses, and can place constraints on the hydration paths for upper tropospheric water.

Greenhouse forcing of surface temperature is significantly influenced by radiative effects of O<sub>3</sub> and H<sub>2</sub>O in the lower stratosphere and around the tropopause [33]. A given fractional change in O<sub>3</sub> has the largest effect on surface forcing when it occurs in the upper troposphere and lower stratosphere [34], but O<sub>3</sub> variations in these regions are poorly characterized. As a consequence, our level of understanding of the greenhouse forcing by stratospheric O<sub>3</sub> changes is now classified as only ‘medium’ [33]. Radiative forcing by stratospheric H<sub>2</sub>O trends is expected to be comparable (and opposite in sign) to that due to O<sub>3</sub> depletion [35]. The important contribution to surface forcing by H<sub>2</sub>O in the near-tropopause region, where its distribution and variation are poorly characterized, has been highlighted in a number of studies. MLS measurements of O<sub>3</sub> and H<sub>2</sub>O will reduce uncertainties in their contributions to future changes.

### C. Pollution in the upper troposphere

Tropospheric pollution and the global effects of regional pollution have received increased attention in the past decade. Aura is making a major step forward with measurements of many tropospheric species by TES. The MLS upper tropospheric measurements complement those from TES. The upper tropospheric region measured directly by MLS exhibits signatures of chemical emissions at the surface, for example from rapid convection and long-range transport processes. Measurements in this region are important for assessing regional impacts on the global atmosphere.

The MLS upper tropospheric measurements (made with varying degrees of precision) include H<sub>2</sub>O, cloud ice, temperature, O<sub>3</sub>, CO, CH<sub>3</sub>CN, and HCN. H<sub>2</sub>O, cloud ice, temperature

and O<sub>3</sub> have sufficient precision for individual profiles to be useful in most situations. Biweekly or monthly maps will probably be the most useful product for CO, CH<sub>3</sub>CN and HCN under normal situations, but single profile measurements are expected to be valuable when the abundances of these species are substantially enhanced, such as can occur in biomass burning episodes. CH<sub>3</sub>CN and HCN are good tracers of biomass burning, and UARS MLS detected a large localized forest fire enhancement of CH<sub>3</sub>CN that was injected into the stratosphere by a strong thunderstorm [36]. An important feature of MLS for studying the upper troposphere is that its measurements can be made in the presence of most ice clouds.

## IV. THE EOS MLS INSTRUMENT

### A. Complement of radiometers

The EOS MLS instrument contains heterodyne radiometers operating at ambient temperature in the five spectral regions given in Table I. The 118 GHz (R1) radiometer, covering the strong 118 GHz O<sub>2</sub> line, was included for temperature and tangent pressure. The 190 GHz (R2) radiometer was included to measure the 183 GHz H<sub>2</sub>O line, as done by UARS MLS, and to measure a strong band of HNO<sub>3</sub> lines. The 240 GHz (R3) radiometer was included to cover very strong O<sub>3</sub> lines in a spectral region where upper tropospheric absorption (mainly by H<sub>2</sub>O vapor) is sufficiently small to allow measurements of upper tropospheric O<sub>3</sub>, and to measure CO. The 640 GHz (R4) radiometer was included to measure the lowest-frequency line of HCl, the strongest rotational line of ClO, and lines of BrO, HO<sub>2</sub> and N<sub>2</sub>O. The 2.5 THz (R5) radiometer was chosen for OH because of the relatively clean spectral region around the pair of strong OH lines at 2.510 and 2.514 THz, and to allow use of a methanol (CH<sub>3</sub>OH) gas laser local oscillator. (Solid state local oscillator systems capable of driving the Schottky diode mixer at 2.5 THz were not available.) The individual radiometers, as indicated in Table I, provide (or contribute to) additional measurements beyond those for which each was included in the instrument. Fig. 4 gives the vertical ranges of chemical species measured by each radiometer.

Planar-technology mixers [37] are used in all the radiometers, with a monolithic millimeter-wavelength integrated-circuit (MMIC) amplifier (e.g., [38]) preceding the mixer in the 118 GHz radiometer. Subharmonically-pumped mixers are in the 118, 190, 240 and 640 GHz radiometers, and fundamental mixers in the 2.5 THz. Local oscillator systems are all solid state, except at 2.5 THz where the gas laser system is used. The MLS THz radiometer is described in [23] and [39].

TABLE I  
EOS MLS RADIOMETERS AND MEASUREMENTS

Radiometer	Primary measurements for which the radiometer was included in EOS MLS	Additional measurements that are provided, or contributed to
R1 (118 GHz)	temperature, pressure	cloud ice, geopotential height
R2 (190 GHz)	H <sub>2</sub> O, HNO <sub>3</sub>	cloud ice, ClO, N <sub>2</sub> O, O <sub>3</sub> , HCN, CH <sub>3</sub> CN, volcanic SO <sub>2</sub>
R3 (240 GHz)	O <sub>3</sub> , CO	cloud ice, temperature, pressure, HNO <sub>3</sub> , volcanic SO <sub>2</sub>
R4 (640 GHz)	HCl, ClO, BrO, N <sub>2</sub> O, HO <sub>2</sub>	cloud ice, O <sub>3</sub> , HOCl, CH <sub>3</sub> CN, volcanic SO <sub>2</sub>
R5 (2.5 THz)	OH	O <sub>3</sub> , cloud ice, temperature, pressure

R3, with better vertical resolution than R1, is expected to eventually provide the primary MLS temperature measurement via the 233.9 GHz <sup>16</sup>O<sup>18</sup>O line.

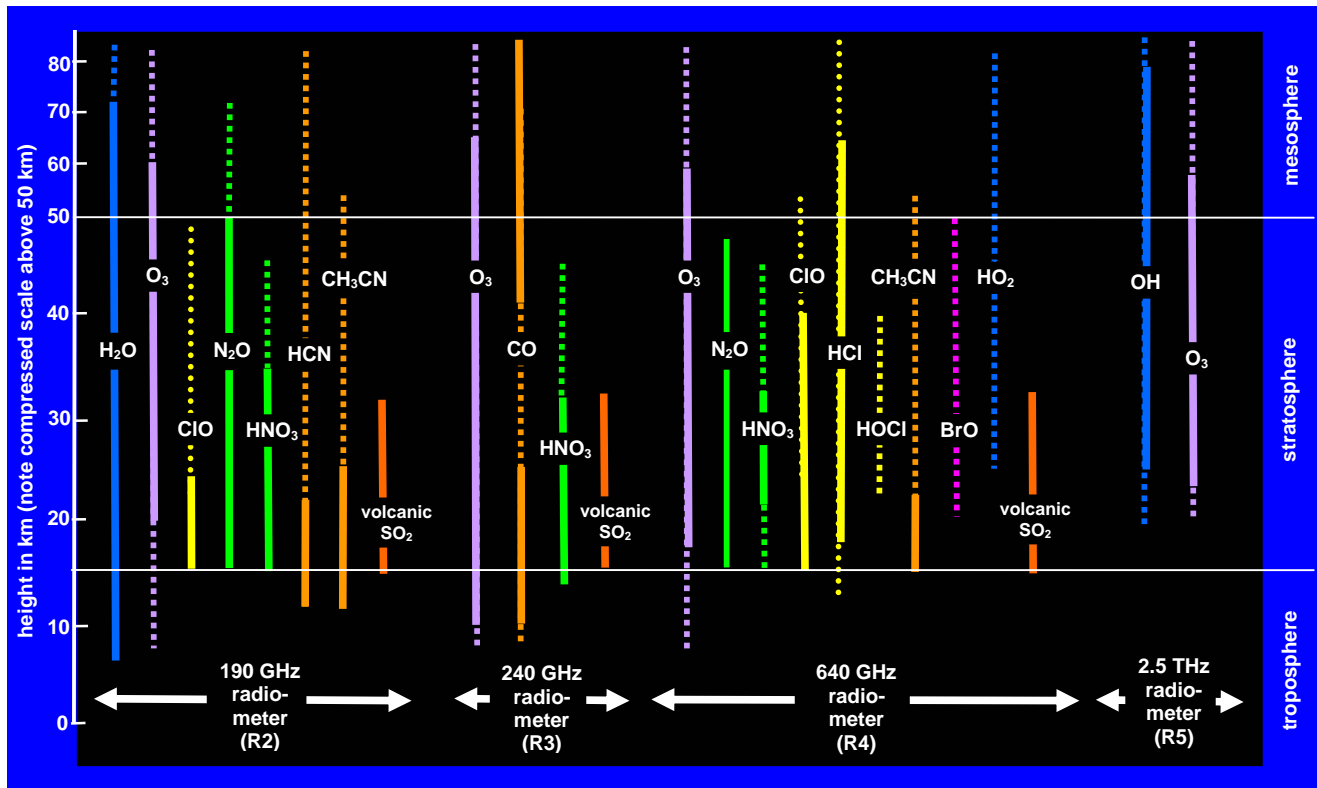


Fig. 4. Chemical species measured by individual EOS MLS radiometers. (All radiometers contribute to measurement of temperature and cloud ice.) Different colors indicate different chemical families. Solid lines indicate generally useful precision for individual profiles. Dotted lines indicate that zonal (or other) averages are generally needed to obtain useful precision. Solid lines for CH<sub>3</sub>CN, HCN and 190 GHz ClO are for enhanced abundances (biomass burning injections of CH<sub>3</sub>CN and HCN, and polar winter vortex ClO). As in Fig. 1, the height ranges shown here indicate what is ultimately expected to be achieved.

*B. Signal flow*

Fig. 5 gives a top-level signal flow block diagram. Atmospheric signals for the 118, 190, 240 and 640 GHz radiometers are collected by a three-reflector offset antenna system that vertically scans the limb. As needed, the antenna can be scanned to high altitudes for a view of ‘cold space’ through the complete antenna system. The GHz antenna design [21] is

similar to that of UARS MLS, with a primary mirror dimension of 1.6 m projected in the vertical direction at the limb tangent point. Atmospheric signals for the 2.5 THz radiometer are obtained via a dedicated telescope and scanning mirror. The 2.5 THz primary mirror dimension in the limb vertical direction is ~25 cm. Sizes of the primary mirrors for both the GHz and THz systems set the FOV widths, as both have diffraction limited designs. Table II gives widths of the fields-of-

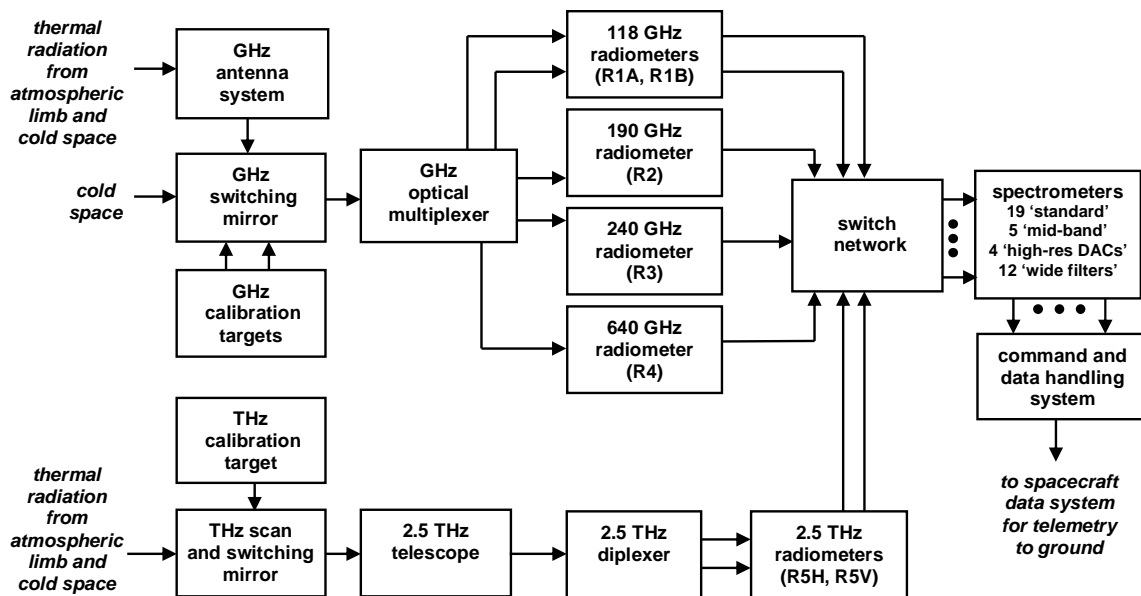


Fig. 5. EOS MLS overall signal flow block diagram.

TABLE II  
EOS MLS FIELD-OF-VIEW WIDTHS

radiometer	vertical (km)	horizontal (km)
R1 (118 GHz)	5.8	12
R2 (190 GHz)	4.2	8.4
R3 (240 GHz)	3.2	6.4
R4 (640 GHz)	1.4	2.9
R5 (2.5 THz)	2.1	2.1

Values are the full width at half power points in the local vertical and horizontal planes at the tangent point. See [21] and [23] for more information.

view at the tangent point for the different radiometers.

A switching mirror following the GHz antenna system provides radiometric calibration by switching to views of on-board blackbody calibration targets or to space. The same calibration targets are used for all GHz bands. There are two GHz calibration targets, although only one (passively cooled to  $\sim 40^\circ\text{C}$  below ambient in orbit, and heated during pre-launch testing) is used during normal in-orbit operations. The second GHz target, included mainly for pre-launch testing, is at ambient temperature. The THz scan mirror, in front of the telescope, provides calibration of the THz bands by rotating to views of cold space and the on-board ambient-temperature THz blackbody calibration target. In normal operation radiometric calibration of all spectral bands is performed between each atmospheric limb scan, every 25 s.

An optical multiplexer, consisting of dichroic plates and a polarization grid arranged as shown schematically in Fig. 6, follows the GHz switching mirror and spatially separates the signal into paths feeding the different GHz radiometers. The second 118 GHz radiometer ('R1B', at the orthogonal polarization) provides redundancy for temperature and pressure. The dichroic plates reflect low frequencies relative to a design value, and transmit high frequencies; the polarization grid reflects one linear polarization and transmits the other.

The radiometers down-convert frequencies of the incoming signals to several broad intermediate frequency (IF) bands in

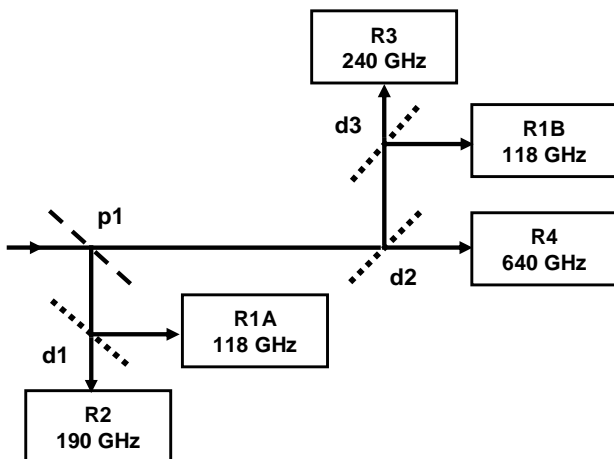


Fig. 6. Schematic of the GHz optical multiplexer. Dichroic plates are indicated by 'dn'; a polarization grid by 'p1'. See [21] for more information.

the range of 3 to 21 GHz. These first IF bands are further down-converted to a common second IF frequency centered at 900 MHz [40]. The broad IF signal bands are fed, via a switch network, to spectrometers that separate the signals into channels for analyses. The switch network gives some redundancy, and can be used to select subsets of measurements in the unexpected event that time-sharing of measurements is required, for example in case of future satellite power limitations.

### C. Spectrometers

Four types of spectrometers, having different spectral resolutions and bandwidths, are used to cover different altitude ranges. Measurements at lower altitudes require more spectral coverage, but less resolution, than those at higher altitudes. 'Standard' 25-channel spectrometers are the primary source of information for measurements throughout the stratosphere. These have a bandwidth of 1300 MHz and resolution varying from 96 MHz at band edges to 6 MHz at band center. Individual channel positions and widths are given in Table III and illustrated in Fig. 7. 'Midband' spectrometers, with filters having the same specifications as the center eleven channels (numbered 8 to 18) in Table III, are used for additional measurements in the middle and upper stratosphere. Digital autocorrelator (DAC) spectrometers provide the finer spectral resolution for measurements of mesospheric temperature,  $\text{H}_2\text{O}$ ,  $\text{O}_3$  and  $\text{CO}$ . These have 129 channels covering 10 MHz width, with a resolution of  $\sim 0.15$  MHz to measure narrow spectral lines at atmospheric pressures below  $\sim 1$  hPa (see Fig. 2). 'Wide' filters, having 0.5 GHz width, extend the spectral range of the

TABLE III  
NOMINAL POSITIONS AND WIDTHS OF FILTERS FOR CHANNELS IN THE MLS 'STANDARD' SPECTROMETERS

channel number	position (MHz)	width (MHz)
1	-575	96
2	-479	96
3	-383	96
4	-303	64
5	-239	64
6	-175	64
7	-119	48
8	-79	32
9	-51	24
10	-31	16
11	-17	12
12	-7	8
13	0	6
14	7	8
15	17	12
16	31	16
17	51	24
18	79	32
19	119	48
20	175	64
21	239	64
22	303	64
23	383	96
24	479	96
25	575	96

Filter positions are relative to the center of the targeted spectral line. Widths are full widths between half power points. The positions and widths for channels 8 to 18 are also the nominal values for channels 1-11 of the MLS 'midband' spectrometers. See [22] for more information.

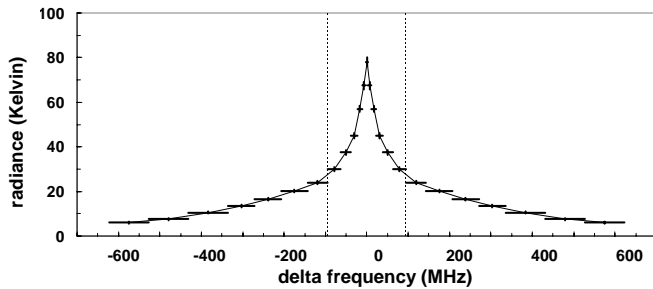


Fig. 7. Illustrating coverage of the EOS MLS ‘standard’ 25-channel spectrometer. Each filter in the spectrometer is shown as a horizontal bar whose width gives the filter resolution. Vertical bars, too small to be seen except in the narrow center channels, give the  $\pm 1\sigma$  noise for the 1/6 s individual integration time of the MLS instrument and a double-sideband radiometer noise temperature of 1000 K. The signal shown here is a simulated ozone line for a limb observation path with tangent height in the lower stratosphere. The 11 filters between the dotted vertical lines also occur in the ‘mid-band’ spectrometers.

25-channel spectrometers for measurements extending lower into the troposphere.

The instrument has 19 ‘standard’ spectrometers, 5 ‘mid-band’ spectrometers, and 4 DAC spectrometers. There are 12 ‘wide’ filters organized into 3 ‘bands’ of 4 channels each (one ‘band’ each in R1A, R1B and R3). All channels of all spectrometers are measured simultaneously and continuously. Table IV gives specifics for all the spectral bands measured by MLS. Fig. 1 of [41] shows the bands superimposed on the atmospheric spectrum.

Digitized data from the spectrometers are passed to the command and data handling system for transmission to the ground. The individual measurement integration time is 1/6 second, termed an MLS Minor Frame (MIF). The MLS Major

Frame (MAF) is the nominal time over which a complete limb scan is taken. A MAF normally has 148 MIFs (120 of which are limb views and the others are calibration views), but occasionally has 149 for synchronization of the limb scan with the Aura orbit.

#### D. Overall instrument

The EOS MLS instrument is fabricated in three modules:

- 1) the ‘GHz module’ that contains the GHz antenna system, calibration targets, switching mirror, optical multiplexer and 118, 190, 240 and 640 GHz radiometers;
- 2) the ‘THz module’ that contains the THz scan and switching mirror, calibration target, telescope and 2.5 THz radiometers at both polarizations;
- 3) the ‘Spectrometer Module’ that contains spectrometers, command and data handling systems, and power distribution systems.

Fig. 8 shows a line drawing and photograph of the instrument. Table V gives overall mass, power and data rate.

#### E. Calibration

The EOS MLS Instrument calibration is described in [21]–[23]. There are four categories:

- 1) ‘Radiometric calibration’ determines the absolute power incident upon the GHz switching mirror, or the THz scan mirror, received through each spectral channel. As typical in microwave radiometry, power is calibrated in terms of a ‘temperature’ that is proportional to the power received, and converges in the long-wavelength limit to the absolute temperature of a blackbody emitting that power. The radiometrically-calibrated outputs are termed ‘radiances’.

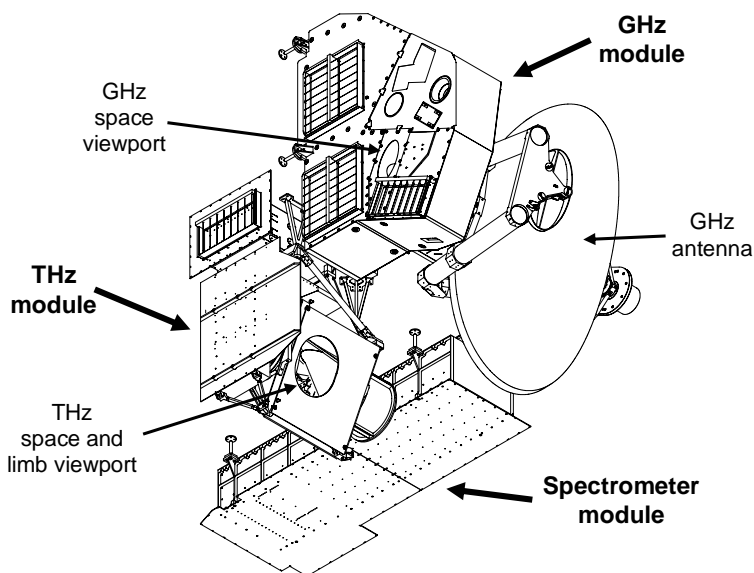


Fig. 8. Line drawing and photograph of the EOS MLS instrument.

TABLE IV  
SPECIFICS FOR SPECTRAL BANDS MEASURED BY EOS MLS.

<sup>a</sup> Radiometer and LO frequency	<sup>b</sup> Primary target molecule	<sup>c</sup> Line rest frequency (GHz)	<sup>d</sup> Band/filter IF center freq.(GHz)	<sup>e</sup> band (or ‘wide filter’) designation	<sup>f</sup> T <sub>sys</sub> (Kelvin)	<sup>g</sup> ΔI <sub>rms</sub> for 1/6 s measurement (kelvin)			<sup>h</sup> ΔI <sub>min</sub> (kelvin)
						@ Δf = 6 MHz	@ Δf = 96 MHz	@ Δf = 500 MHz	
<b>R1 (A&amp;B)</b> <b>118 GHz</b> 126.800 (÷2 = 63.400)	O <sub>2</sub> wing		-11.5	B32W.C1 (A)	1100			0.2	0.1
	O <sub>2</sub> wing		-11.5	B34W.C1 (B)	1400			0.2	0.1
	O <sub>2</sub> wing		-9.8	B32W.C2 (A)	1000			0.1	0.1
	O <sub>2</sub> wing		-9.8	B34W.C2 (B)	1100			0.2	0.1
	O <sub>2</sub>	*118.7503	-8.0470	B1F, B22D	1200	1.2	0.3		0.1
	O <sub>2</sub> wing		-6.3	B32W.C3 (A)	1100			0.2	0.1
	O <sub>2</sub> wing		-6.3	B34W.C3 (B)	1200			0.2	0.1
	O <sub>2</sub> wing O <sub>2</sub> wing		-4.8	B32W.C4 (A)	1500			0.2	0.1
			-4.8	B34W.C4 (B)	1600			0.3	0.1
<b>R2</b> <b>190 GHz</b> 191.900 (÷2 = 95.950)	H <sub>2</sub> O	183.3101	-8.5858	B2F, B23D	1100	1.1	0.3		0.05
	N <sub>2</sub> O	200.9753	9.0798	B3F	1100	1.1	0.3		0.05
	HNO <sub>3</sub>	181.5946	-10.3013	B4F	1000	1.0	0.3		0.05
	ClO	*204.352	12.4566	B5F	950	1.0	0.3		0.02
	O <sub>3</sub>	206.1320	14.2367	B6F	900	0.9	0.2		0.05
	HCN	177.2612	-14.6348	B27M	900	0.9	0.2		0.05
<b>R3</b> <b>240 GHz</b> 239.660 (÷2 = 119.830)	O <sub>3</sub> wing		+/- 3.0	B33W.C1	1200			0.2	0.05
	O <sub>3</sub>	235.7098	-3.9449	B7F, B24D	1400	1.4	0.4		0.05
	O <sub>3</sub> wing		+/- 4.8	B33W.C2	1500			0.2	0.05
	<sup>18</sup> OO	233.9462	-5.7085	B8F	1600	1.6	0.4		0.05
	O <sub>3</sub> wing		+/- 7.2	B33W.C3	1300			0.2	0.05
	O <sub>3</sub> wing		+/- 7.8	B33W.C4	1300			0.2	0.05
	CO	230.5380	-9.1168	B9F, B25D	1200	1.2	0.3		0.05
<b>R4</b> <b>640 GHz</b> 642.870 (÷2 and ÷3 = 107.145)	ClO	*649.4512	6.5959	B10F	4200	4.2	1.1		0.05
	HO <sub>2</sub>	649.7015	6.8462	B28M	4400	4.4	1.1		0.05
	HOCl	635.8700	-6.9856	B29M	4400	4.4	1.1		0.05
	<sup>81</sup> BrO	*650.179	7.3237	B11F	4400	4.4	1.1		0.05
	N <sub>2</sub> O	652.8338	9.9785	B12F	4300	4.3	1.1		0.05
	HCl	*625.9188	-16.9373	B13F	4000	4.0	1.0		0.05
	O <sub>3</sub>	625.3715	-17.4844	B14F	4000	4.0	1.0		0.05
	HO <sub>2</sub>	660.4857	17.6306	B30M	4100	4.1	1.0		0.05
	<sup>81</sup> BrO	*624.768	-18.0879	B31M	4100	4.1	1.0		0.05
<b>R5 (V&amp;H)</b> <b>2.5 THz</b> 2522.7816	OH (H)	*2514.316	-8.4081	B15F	13000	13	3.3		0.1
	OH (V)	*2514.316	-8.4081	B18F	11000	10	2.5		0.1
	OH (H)	*2509.949	-12.7759	B16F	13000	13	3.3		0.1
	OH (V)	*2509.949	-12.7759	B19F	11000	10	2.5		0.1
	O <sub>2</sub> (H)	*2502.323	-20.4012	B17F	18000	18	4.5		0.1

<sup>a</sup>The R1 and R5 LO frequencies were chosen for engineering considerations; others were chosen to target measurements in both sidebands. R1 is single sideband and others are double sideband. There are two nominally identical radiometers (having orthogonal polarizations) for R1, with R1B included for redundancy. There are also two orthogonally-polarized radiometers for R5, to improve quality of the OH measurement. The ‘(÷ 2 = f)’ below the LO frequency gives the frequency *f* of the fundamental oscillator used to generate the LO. There is an additional ÷ 3 for the 640 GHz radiometer where a frequency-tripler is used, as well as its mixer being subharmonically pumped like the 118, 190 and 240 GHz radiometers.

<sup>b</sup>R2 and R4 also measure CH<sub>3</sub>CN and R3 also measures HNO<sub>3</sub>; all radiometers contribute to the cloud ice measurement.

<sup>c</sup>Spectral lines with fine structure are marked by \*. There are several strong O<sub>3</sub> lines in both sidebands of R3 near the 235 GHz O<sub>3</sub> line listed here.

<sup>d</sup>IF center frequencies are after first down-conversion of frequency, and account for line-of-sight orbital motion Doppler shift of the spectral lines. Negative indicates the target measurement is in the radiometer lower sideband, and ± indicates targeted measurements in both upper and lower sidebands. There is further downconversion to center the target at 900 MHz for the ‘standard’ filter banks, then to 200 MHz for the ‘mid-band’ filter positions, and then to 5 MHz for the digital autocorrelator spectrometers.

<sup>e</sup>Bn indicates MLS spectral band n. BnF indicates a ‘standard’ 25-channel filter bank, BnM indicates an 11-channel ‘mid-band’ filter bank, BnD indicates a high-resolution digital autocorrelator. BnW.Cm indicates a wide filter (channel m of band n). The standard operational deployment of spectrometers is shown here.

<sup>f</sup>T<sub>sys</sub> is the ‘system noise temperature’ for the band or channel. This is a single-sideband value for R1, which is a single (lower) sideband radiometer. It is a double-sideband value for R2-R5. See [22] and [23] for more information.

<sup>g</sup>ΔI<sub>rms</sub> is the rms noise in the spectrally-varying component of the calibrated radiance, and for values down to ~ΔI<sub>min</sub> is given approximately by T<sub>sys</sub>/sqrt(Bτ), where B is the noise bandwidth and τ is integration time for which the measurement is accumulated, with broader channels having somewhat larger noise. See [22] and [23] for more information.

<sup>h</sup>ΔI<sub>min</sub> is the minimum spectrally-varying component of the radiance that is required for measurement.

TABLE V  
EOS MLS OVERALL MASS, POWER AND DATA RATE

mass	power	data rate
453 kg	545 W	100 kb/s

<sup>a</sup>Value is for full-up operation, including the R1B ‘redundant’ 118 GHz radiometer, and is the average over a two-orbit period.

- 2) ‘Field-of view calibration’ determines the relative response of the instrument as a function of the angle at which the input signal is incident upon the antenna.
- 3) ‘Spectral calibration’ determines the relative response as a function of the frequency of the input signal.
- 4) ‘Engineering calibration’ gives the output of engineering sensors in appropriate units (e.g., volts, amperes).

Approximate accuracies of the radiometric, spectral and field-of-view calibrations [21]-[23] are:

- 1) Radiometric: The systematic uncertainty in the atmospheric/Earth radiances measured through each spectral channel is less than :
  - (a) 3 K for the absolute value of the radiances, and
  - (b) 1% or  $\Delta I_{\min}/3$  for the spectrally-varying component of the radiances measured from one channel or filter to another throughout a given radiometer, where  $\Delta I_{\min}$  for each spectral region is given in Table IV.
- 2) Spectral and field-of-view: The spectral and FOV responses are characterized sufficiently that their separate uncertainties do not introduce uncertainties in the MLS ‘forward model’ calculations of the atmospheric/Earth radiances of more than:
  - (a) 3 K in the absolute value of radiances measured through each spectral channel, and
  - (b) 1% or  $\Delta I_{\min}/3$  for the spectrally-varying component of the radiances measured from one channel or filter to another throughout a given radiometer.

To ensure efficient scanning of the vertical region of interest, the accuracy in placement of the tangent height of the FOV boresights, after in-orbit adjustments, is  $\pm 0.5$  km at the start of each limb scan (which can degrade to  $\pm 1$  km at the end of the limb scan). To ensure that tangent height uncertainties due to boresight elevation uncertainties are comparable to, or less than, the equivalent height uncertainties in MLS measurements of tangent pressure, the changes in elevation of the FOV boresights with respect to nadir during each limb scan are known to  $\sim 2$  arcsecond, and the rate of change is known to  $\sim 1$  arcsecond per second at time scales between 1/6 and 25 seconds. MLS instrument data on the FOV boresight elevation, and spacecraft data relevant to the MLS FOV boresight elevation, are recorded at least twice per MIF. Jitter in elevation of the FOV boresights at time scales shorter than 1/6 s, as determined from analyses of pre-launch data, is  $\sim 8$  arcseconds peak-to-peak and caused dominantly by performance of the MLS pointing control system [21]. This jitter integrates down to give 1 arcsecond FOV boresight uncertainty for each 1/6 s MLS individual measurement. Absolute pointing knowledge, needed for the geopotential height measurements, is obtained from the Aura satellite star tracker and Inertial Reference

Unit. Drifts in these data can be ‘calibrated out’ by analyses of overlapping observations from successive orbits in the polar regions, and in the tropics where MLS temperature data indicate stable atmospheric conditions.

## V. MEASUREMENT COVERAGE

The Aura orbit is sun-synchronous at 705 km altitude with  $98^\circ$  inclination, 1:45 p.m. ascending (north-going) equator-crossing time, and 98.8 minute period. The MLS fields-of-view ‘look’ in the forward direction (direction of orbital motion) and vertically scan the limb in the orbit plane. This gives  $82^\circ\text{S}$  to  $82^\circ\text{N}$  latitude coverage on each orbit. The mean geometric distance to the atmospheric limb, for 6371 km mean Earth radius, is  $\sim 3080$  km for 10 km tangent height ( $-25.61^\circ$  elevation angle) and  $\sim 2970$  km for 50 km tangent height ( $-24.75^\circ$  elevation angle). The limb is scanned in the upward direction to give an observation path tangent point locus that is much more vertical (see Fig. 1 of [42]) than if the limb were scanned downward. The higher tangent points are closer to the satellite, which the forward motion compensates for in the Earth frame of reference.

In nominal operation the MLS limb scans are synchronized to the orbit, with 240 scans per orbit and phased such that limb scan tangent point loci occur near the equator on each equator crossing. This gives  $1.5^\circ$  (165 km, 24.7 s) along-track separation between adjacent limb scans, which is well-matched to the along-track resolution for upper tropospheric water vapor measurements. There are equal numbers of limb scans in the northern and southern hemisphere. Fig 9 illustrates the operational limb scan profiles that have been used to date since launch; Table VI gives details. These scans are performed continuously (non-stepped), and the 1/6 s integration time provides upper tropospheric and lower stratospheric radiance measurements every 0.3-0.5 km in the vertical. MLS obtains vertical profiles at 3500 locations over the globe every 24 hours.

Fig. 10 shows the locations of the limb scans for one 24-hour period. As the Aura orbit is sun-synchronous, MLS observations at a given latitude on either the ascending or descending sides of the orbit have approximately the same local solar time (to within several minutes) throughout the mission.

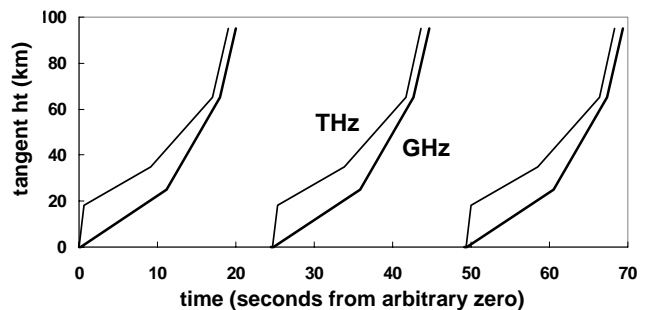


Fig. 9. EOS MLS operational limb scan profiles. The curves give the tangent point height of the FOV boresights as a function of time. Radiometric calibration (observation of blackbody target and of cold space) and FOV retrace are performed in the gap between limb scans. The  $\sim 1$  s difference between the ends of the THz and GHz scans is to reduce power transients when mirrors move quickly during retrace.

TABLE VI  
DETAILS OF THE NOMINAL GHZ AND THZ LIMB SCANS

GHZ scan				THz scan			
tangent height range (km)	MIF range	rate (deg/s)	rate (km/MIF)	tangent height range (km)	MIF range	rate (deg/s)	rate (km/MIF)
0-25	1-67	0.0422	0.37	0-18	1-4	0.510	4.50
25-65	68-108	0.110	0.98	18-35	5-55	0.0375	0.33
65-95	109-120	0.270	2.5	35-65	56-102	0.072	0.64
switching mirror at space view; antenna retrace	123-135	not applicable	not applicable	65-95	103-114	0.270	2.50
switching mirror at target view; antenna retrace	138-144	not applicable	not applicable	120-154 (23.3° space view)	118-128	not applicable	not applicable
return to 0 km limb view	145-147	not applicable	not applicable	target view	132-138	not applicable	not applicable
				<sup>a</sup> return to 0 km limb view	139-147	not applicable	not applicable

The MLS major frame (MAF) length is usually 148 MIFs (24.67 s), but occasionally is 149 MIFs (24.83 s) to synchronize the MLS scan to the orbit. MIF numbering starts at 0; MIF 0 (and 148 when present) is at 0 km tangent height. Missing MIF numbers in this table are where mirrors are moving.

<sup>a</sup>The THz mechanism spends MIFs 142-147 searching for zero encoder index while moving the FOV at ~1 deg/s near or below 0 km tangent height; this period provides useful information on cloud ice.

Fig. 11 shows the local solar time of the measurements as a function of latitude.

VI. DATA PROCESSING AND PRODUCTS

There are three levels of MLS data processing that produce corresponding levels of data products as summarized in Table VII. The EOS MLS data processing system is described in [43]

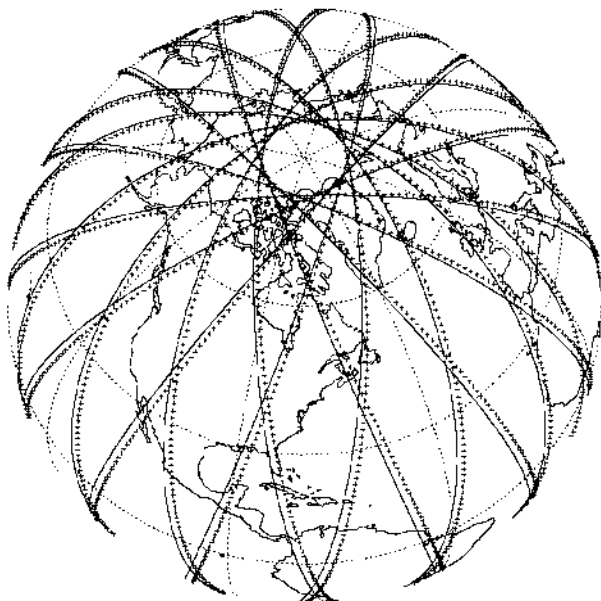


Fig 10. EOS MLS measurement locations (crosses) for a 24 hour period. The suborbital track (continuous line) is slightly displaced because of Earth's rotation during the time the satellite moves forward to the MLS tangent point latitude. The ascending (mostly daytime) portions of the orbit are those with the southeast-northwest tilt.

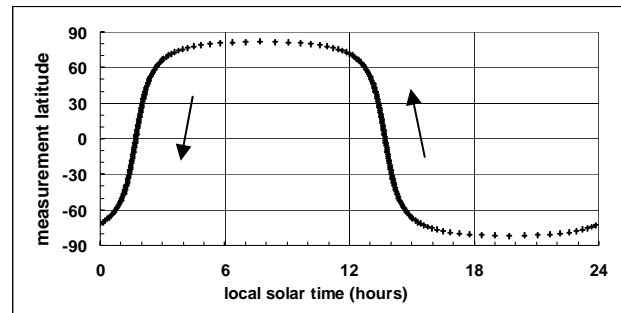


Fig. 11. Local solar time of MLS measurements versus latitude. Crosses give locations of profile measurements. Arrows show the direction of motion around the orbit.

TABLE VII  
MLS DATA

Level	Primary contents	Daily volume (Mbytes)
0	raw data from instrument	~1000
1	calibrated and geo-located radiances and engineering data	~4000
2	retrieved geophysical parameters and diagnostics	~1000
3	mapped and gridded data, daily/monthly zonal means	~100

Volumes given are for the archived products. Level 1 and 2 data files are produced on a daily basis, with each daily file for 00-24 hours UT; Level 3 data will be produced on a monthly basis, with equivalent daily volumes given here. The MLS Level 1 data are sometimes referred to as 'Level 1B', to distinguish them from 'Level 1A' datasets that do not include geo-location.

### A. Level 1 Processing

EOS MLS Level 1 data processing algorithms are described in [22] and [23]. The primary tasks are to:

- 1) qualify each raw input datum using instrument configuration and checksum data, as well as transmission quality flags and statistical tests for ‘reasonableness’,
- 2) calibrate the instrument engineering data (e.g., voltages and temperatures),
- 3) interpolate space and target radiometric measurements to the time of the limb measurements,
- 4) calculate radiometric gain at the time of the limb measurements,
- 5) estimate components of the limb signal arising from antenna emission and scattering effects,
- 6) calibrate the limb radiances and provide estimates of their uncertainties,
- 7) determine the field-of-view boresight pointing angles for each radiometer,
- 8) generate ancillary data (e.g., tangent point location, local solar time and zenith angles; flags for ‘bright objects’ in the field-of-view) that are needed for quality checks in Level 2 processing, and
- 9) produce daily files of the data and a log summarizing instrument performance and outputs.

The calibrated radiances produced by Level 1 processing are the values, for each spectral channel and 1/6 s instrument integration period, of the radiance received within approximately  $6^\circ$  of the field-of-view boresight direction. This is the angular range  $\Omega_a$  over which the shape of the field-of-view is measured during ground calibrations, and for which radiances are calculated in Level 2 processing. The small amount of radiance received outside  $\Omega_a$  is estimated and removed during Level 1 processing. The radiance is calibrated as average radiant power per unit spectral interval received by that channel, and is expressed in units of temperature as discussed earlier.

Inputs to Level 1 processing are (a) the MLS Level 0 data, (b) the Aura satellite ephemeris and engineering data that are used, for example, to obtain satellite location and attitude, and (c) solar, lunar and planetary ephemerides, which are used to ‘flag’ situations when objects (e.g., moon, planets) are in the MLS fields-of-view.

### A. Level 2 Processing

Primary tasks of the Level 2 processing are to:

- 1) retrieve boresight tangent pressures and geophysical parameters (such as temperature and constituent abundances) from the EOS MLS Level 1 data, and give estimated uncertainties for the retrieved quantities;
- 2) produce diagnostic information (such as radiances calculated from the retrieved parameters, and chi-square statistics) on the quality of the retrieved geophysical parameters, and ‘flags’ to identify bad retrievals;
- 3) Produce ancillary data, such as tropopause pressure, which may be derived from MLS data and/or ancillary

meteorological data available at the time of data processing; and

- 4) produce daily files of the output data, and a log summarizing appropriate information on the processing statistics for that day.

Table VIII lists the ‘standard’ geophysical data product output files produced by Level 2. Table IX gives the contents of the Level 2 geophysical data quantities ‘diagnostic’ file. Typical ‘diagnostic’ quantities are species atmospheric profiles retrieved from spectral regions other than that used for the standard product for that species. These quantities provide valuable cross-checks for the retrieved quantities.

MLS Level 2 data processing algorithms are described in [42], and simultaneously retrieve atmospheric structure in both the vertical and line-of-sight direction [44]. The ‘forward models’ used by this processing are described in [41] and [45], and algorithms for the MLS cloud measurements in [46].

The standard MLS vertical grid, used for retrievals of most geophysical parameters, represents the atmospheric profile as a piecewise-linear function of the logarithm of atmospheric pressure, with breakpoints at  $10^{-n/6}$  hPa ( ... , 0.316, 0.464, 0.681, 1.00, 1.47, 2.15, 3.16, ... ). Under normal operation, profiles are retrieved every  $1.5^\circ$  of great circle arc along the suborbital path. Where needed, ‘smoothing’ (in the vertical and/or horizontal directions) is implemented to stabilize the retrieved profile at the expense of degraded resolution. The geophysical data product output files also contain the estimated precision for each datum. Precision is set negative when the retrieved value has more than  $\sim 25\%$  contribution from the *a priori*. A ‘quality’ indicator that indicates the degree to which (in a chi-square sense) the appropriate radiances are fitted by the retrievals, and a ‘status’ flag to indicate ‘abnormalities’ (such as operational abnormalities), are included for each retrieved profile for each product. See [42] and [47] for more information.

Inputs to the Level 2 processing are MLS Level 1 data and operational meteorological data from GMAO (NASA’s Global Modeling and Assimilation Office) or, if needed, can be from NCEP (National Centers for Environmental Prediction).

### B. Level 3 Processing

Primary tasks of MLS Level 3 processing, not yet operational, are to produce:

- 1) daily maps for data having adequate signal-to-noise,
- 2) daily and monthly zonal means, and
- 3) monthly gridded maps.

Algorithms for producing the daily maps are described in [48]. Fourier ‘asynoptic mapping’ techniques, as initially developed by [49], are used to produce the maps from the MLS Level 2 data files. Table X gives the planned MLS Level 3 data products.

## VII. SOME INITIAL RESULTS

Following launch on 15 July 2004, activation of the MLS instrument began on 18 July. ‘First light’ with the THz module was achieved on 24 July; with the GHz module on 27 July.

TABLE VIII  
MLS LEVEL 2 ‘STANDARD’ GEOPHYSICAL DATA PRODUCT FILES

measurement (alphabetical order)	Filename	Units	<sup>a</sup> Initial vertical range of retrieval			
			pressure (hPa)		~height (km)	
			max	min	max	min
BrO	ML2BRO	vmr	147	0.001	13	95
ClO	ML2CLO	vmr	147	0.001	13	95
CO	ML2CO	vmr	316	0.001	8	95
<sup>b</sup> CH <sub>3</sub> CN	ML2CH3CN	vmr	316	0.001	8	95
geopotential height	ML2GPH	m	316	0.001	8	95
H <sub>2</sub> O	ML2H2O	vmr	316	0.001	8	95
HCl	ML2HCL	vmr	147	0.001	13	95
HCN	ML2HCN	vmr	100	0.001	15	95
HNO <sub>3</sub>	ML2HNO3	vmr	316	0.001	8	95
HO <sub>2</sub>	ML2HO2	vmr	147	0.001	13	95
HOCl	ML2HOCL	vmr	147	0.001	13	95
ice water content of clouds	ML2IWC	mg/m <sup>3</sup>	316	46	8	20
N <sub>2</sub> O	ML2N2O	vmr	215	0.001	11	95
O <sub>3</sub>	ML2O3	vmr	316	0.001	8	95
OH	ML2OH	vmr	68	0.001	18	95
relative humidity w.r.t. ice	ML2RHI	percent	316	0.001	8	95
<sup>c</sup> SO <sub>2</sub>	ML2SO2	vmr	215	0.1	11	65
temperature	ML2T	kelvin	316	0.001	8	95

Each of the data files listed here is ~3 Mbyte in size, except for temperature, which is ~6 Mbyte.

<sup>a</sup>The retrieval vertical range generally extends beyond the range for which the data are expected to be useful. Ranges given here are for MLS Version 1.5 data.

<sup>b</sup>CH<sub>3</sub>CN is not an initial standard data product, but is expected eventually to be so.

<sup>c</sup>SO<sub>2</sub> is retrieved ‘off-line’ in Version 1.5 data; an SO<sub>2</sub> ‘standard’ data product file can be produced when it is detected.

TABLE IX  
MLS LEVEL 2 GEOPHYSICAL DATA DIAGNOSTIC QUANTITIES

Quantity	Brief description
spectral baselines	retrieved values for various instrumental ‘spectral baselines’
CH <sub>3</sub> CN-190	CH <sub>3</sub> CN from the ‘Core+R2’ retrieval phase
CH <sub>3</sub> CN-640	CH <sub>3</sub> CN from the ‘Core+R4’ retrieval phase
ClO-190	ClO from the ‘Core+R2’ retrieval phase
ClO-640	ClO from the ‘Core+R4’ retrieval phase
H <sub>2</sub> O-190	H <sub>2</sub> O from the ‘Core+R2’ retrieval phase
H <sub>2</sub> O-Core	H <sub>2</sub> O from the ‘Core’ retrieval phase
H <sub>2</sub> O-InitUTH	H <sub>2</sub> O from the ‘Init UTH’ portion of the ‘Core’ retrieval phase
HNO <sub>3</sub> -190	HNO <sub>3</sub> from the ‘Core+R2’ retrieval phase
HNO <sub>3</sub> -240	HNO <sub>3</sub> from the ‘Core+R3’ retrieval phase
HNO <sub>3</sub> -640	HNO <sub>3</sub> from the ‘Core+R4’ retrieval phase
IWC-190	ice water content from the ‘Core+R2’ retrieval phase
IWC-240	ice water content from the ‘Core+R3’ retrieval phase
IWC-640	ice water content from the ‘Core+R4’ retrieval phase
N <sub>2</sub> O-190	N <sub>2</sub> O from the ‘Core+R2’ retrieval phase
N <sub>2</sub> O-640	N <sub>2</sub> O from the ‘Core+R4’ retrieval phase
O <sub>3</sub> -190	O <sub>3</sub> from the ‘Core+R2’ retrieval phase
O <sub>3</sub> -240	O <sub>3</sub> from the ‘Core+R3’ retrieval phase
O <sub>3</sub> -640	O <sub>3</sub> from the ‘Core+R4’ retrieval phase
O <sub>3</sub> -UpdatePtan	O <sub>3</sub> from the ‘UpdatePtan’ portion of the ‘Core’ retrieval phase
refGPH-<various>	reference geopotential height from various phases of the retrievals
RHI-190	relative humidity from ‘Core+R2’ retrieval phase
RHI-Core	relative humidity from ‘Core’ retrieval phase
RHI-InitUTH	relative humidity from the ‘InitUTH’ portion of ‘Core’
Temperature-<various>	temperature from various phases of the retrievals
tpPressure-wmo	tropopause pressure, based on WMO definition of tropopause
numeric diagnostics	diagnostics on or from Level 2 numerical problem solvers

TABLE X  
 PLANNED MLS LEVEL 3 DATA PRODUCTS

Planned product filename	Brief description	Time interval for each file	Volume (Mbyte)
ML3D<XX>	Gridded daily maps: separate file for each Level 2 product XX for which a Level 3 map is produced	1 day	varies from 3.5 to 14,
ML3DSPC	Wave spectra for each map: amplitude and phase, for each latitude and pressure level, of the Fourier components fitted to the Level 2 data.	10 days (centered on ~30 days of Level 2 data)	~500 total, average ~35 for each product
ML3MMAFS	Gridded monthly map 'standard' file: monthly maps for all products	1 month	~40
ML3MMAFD	Monthly map 'diagnostic' file: diagnostics for all products	1 month	~50
ML3DZMS	Daily zonal mean 'standard' file: daily zonal means for all products	1 day	~3
ML3DZMD	Daily zonal mean 'diagnostic' file: diagnostics for all products	1 day	~5
ML3MZMS	Monthly zonal mean 'standard' file: monthly zonal means for all products	1 month	~3
ML3MZMD	Monthly zonal mean 'diagnostic' file: diagnostics for all products	1 month	~5

Fig. 12 shows 'first light' spectra from radiometers in each of the five MLS broad spectral regions measured at tangent heights in the middle to upper stratosphere; these illustrate the excellent performance of the instrument from the start of observations. The first full day of operation in orbit was 3 August 2004, and full-up science operations began on 13 August.

MLS operations started in time to observe development of the 2004 Antarctic ozone hole [50], and its breakup [51]. Fig. 13 shows 3 August 2004 measurements over Antarctica that are relevant to polar processes affecting ozone. At this time of year sunlight is returning to the south polar region and rapid ozone loss is just beginning. MLS provides an extensive data set for tracking polar processes affecting stratospheric ozone. These are especially valuable for the Arctic, where climate change could cause increased ozone loss.

Fig. 14 shows MLS measurements of OH and HO<sub>2</sub> made on 30 August 2004. This illustrates the MLS ability to make these new measurements (on a daily basis for zonal means), and the wide dynamic range, from 10<sup>-12</sup> to 10<sup>-9</sup> relative abundances, over which they can be made. Initial validation of the OH and HO<sub>2</sub> measurements with balloon instruments, and some early results relative to the 'HO<sub>x</sub> dilemma' are given in [52]. Solar proton flare enhancement of mesospheric OH and HO<sub>x</sub>, and the resulting effects on O<sub>3</sub> have also been detected [53]. The most difficult stratospheric measurement for MLS is BrO, which is generally expected to require monthly averages for useful precision. Fig. 15 shows spectra for the two

BrO lines observed by MLS, as well as the spectra for some other relatively weak lines, measured on 3 August 2004. The quality of these spectra shows that useful measurements of all these species are being obtained.

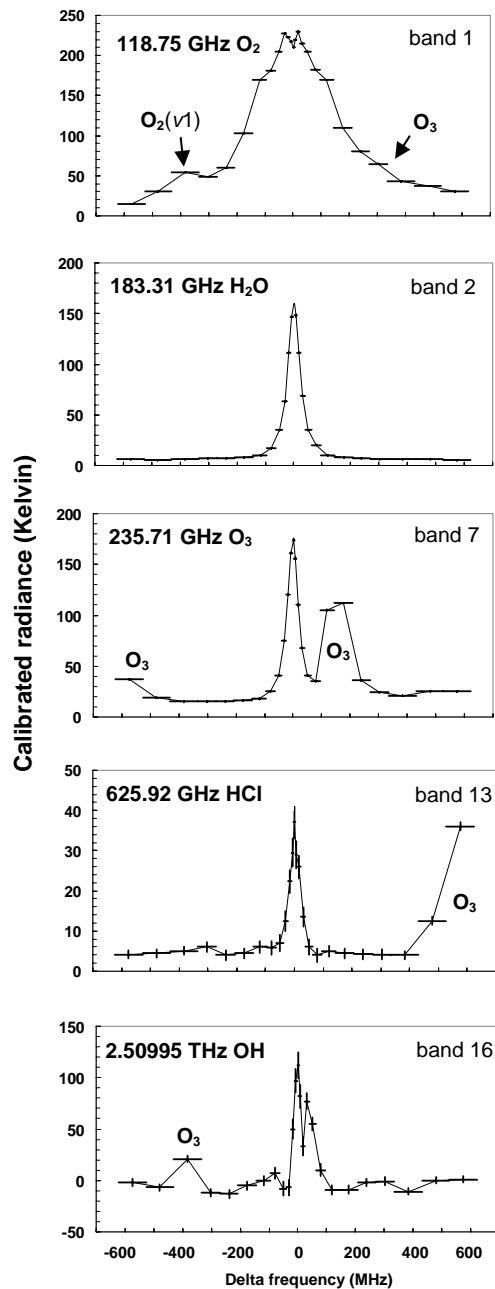


Fig. 12. Examples of target spectral lines measured by five different MLS radiometers and 'standard' 25-channel spectrometers. The target line, centered in the band, is labeled in the upper left of each panel. Additional lines of O<sub>3</sub> evident in some bands, and the vibrationally-excited O<sub>2</sub> line in band 1 are indicated. The two fine structure components for OH are easily seen, and the three for HCl can be seen with more scrutiny. These are EOS MLS 'first light' measurements: OH on 24 July 2004, the others on 27 July. Vertical bars (too small to be seen in many cases) give  $\pm 1\sigma$  noise for the individual 1/6 s measurements; horizontal bars give individual filter widths.

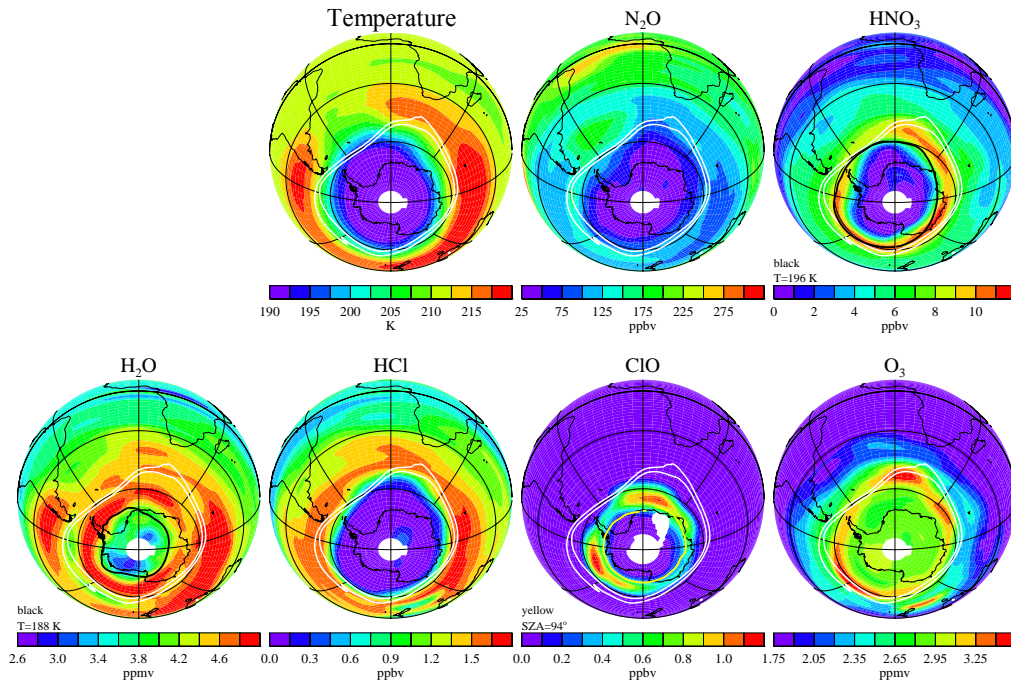


Fig. 13. MLS measurements on 3 August 2004 for ~18 km height (lower stratosphere, interpolated to the 490 K potential temperature isentropic surface). White contours, potential vorticity from operational meteorological data, indicate the dynamical edge of the Antarctic vortex. Vortex temperatures are low; values of  $N_2O$  are also low, characteristic of air that has descended from higher altitudes. Descending air also brings large values of  $HNO_3$  and  $H_2O$ . In the coldest regions of the vortex (black contours),  $HNO_3$  and  $H_2O$  are depleted by formation of polar stratospheric clouds. Reactions on these clouds trigger conversion of chlorine from the reservoir HCl to ozone-destroying ClO. The yellow contour on ClO (shown on day side of the orbit only) indicates the edge of daylight, required for substantial amounts of ClO. See [50] and [51] for analyses of the evolution of these quantities during development and breakup of the 2004 Antarctic ozone hole.

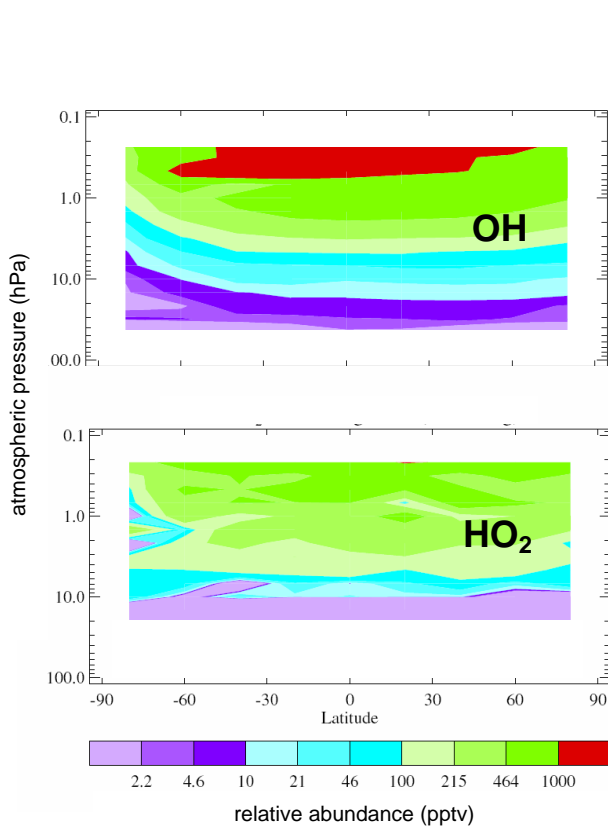


Fig. 14. OH and  $HO_2$  measured on 30 Aug. 2004. Zonal means from the ascending (day) side of the orbit are shown.

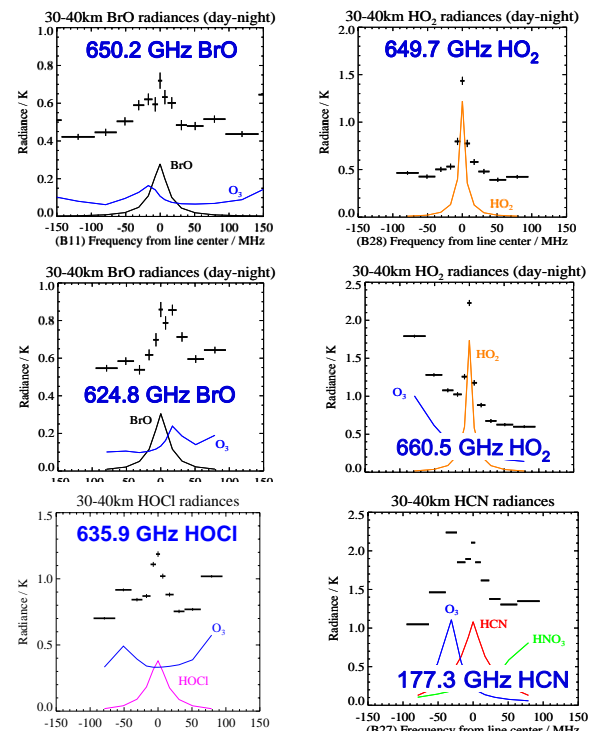


Fig. 15. Spectra for weaker signals observed by MLS. Global averages of measurements made at ~30-40 km tangent heights on 3 Aug 2004 are shown; the targeted spectral line is labeled in each panel. Vertical extents of bars give the estimated noise for the average; horizontal extents show the spectral resolution of each filter. Smooth curves give calculated spectra for species in the band. Zero levels on the vertical axes, and offsets of calculated spectra, are arbitrary.

Measurements of carbon monoxide (CO) in an upper stratospheric layer at  $\sim 50$  km altitude are shown in Fig. 16. CO is a good tracer of atmospheric air masses. In the upper stratosphere and mesosphere it traces descent of CO-rich air produced by photodissociation of  $\text{CO}_2$  in the thermosphere. In the upper troposphere CO traces injections of polluted air from below. Enhanced abundances of CO in the upper troposphere over southern Asia have been detected by MLS [54]. These are consistent with chemical model results that show the enhanced CO originated from surface pollution in industrial regions of southern Asia [55].

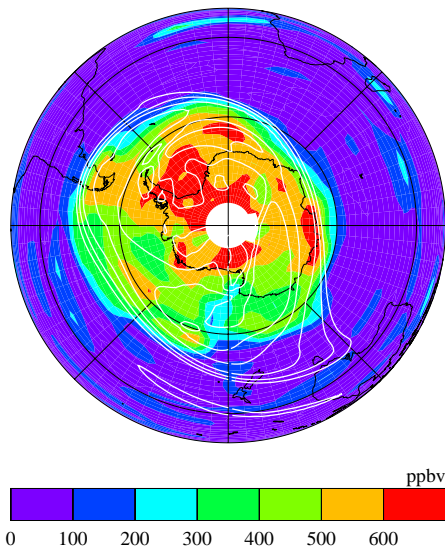


Fig. 16. Carbon monoxide in a layer at  $\sim 50$  km altitude measured on 3 August 2004. White contours are potential vorticity (from operational meteorological data), where closely spaced contours indicate the dynamical edge of the Antarctic winter vortex.

EOS MLS is continuing the UARS MLS measurements of upper tropospheric water vapor [9]-[11] and cloud ice [12], but with much better resolution and sensitivity. The improvements over UARS are due to the EOS MLS denser vertical and horizontal sampling in the upper troposphere, and its broader spectral bandwidth. Fig. 17 shows an example of the EOS MLS upper tropospheric  $\text{H}_2\text{O}$  measurements. Fig. 18 shows an example of the cloud ice measurement. Comparisons of the MLS cloud ice measurements with operational analyses products and global circulation models are given in [56]. Information on cirrus crystal orientation has been obtained from the dual polarization measurements of the R1A and R1B radiometers [57]. The broad spectral range of EOS MLS also contains information on the size distribution of cloud ice particles [58]. Injections of  $\text{SO}_2$  into the stratosphere have been detected [59] from the New Guinea Manam volcano that erupted on 27 January 2005. Line-of-sight mesospheric wind has also been obtained from research algorithms [60], and compared with other measurements in analyses of the “two-day wave” in the mesosphere [61].

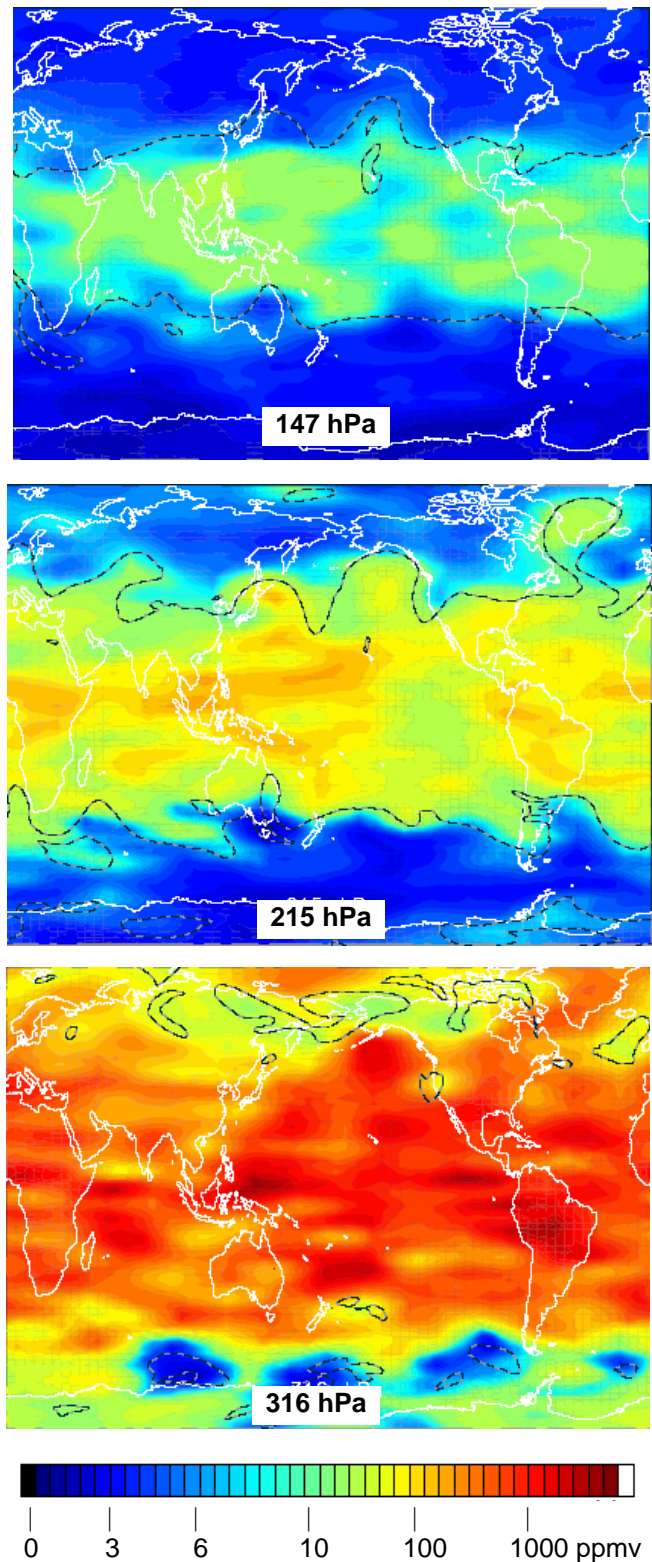


Fig. 17. EOS MLS measurements of upper tropospheric water vapor at three pressure heights on 20 October 2004. The dashed contours are values of potential vorticity (from operational meteorological data) that are representative of the tropopause, which generally separates dry stratospheric air from moist tropospheric air.

## VIII. VERSION 1.5 DATA

In January 2005, the EOS MLS Science Data Processing System [43] began producing the first version of MLS data being made publicly available. These algorithms and data version, denoted MLS ‘Version 1.5’ (v1.5), include improvements implemented as a result of inspecting the data produced by preliminary algorithms used immediately after launch. A ‘data quality document’ [47] describes the quality of each MLS geophysical data product, including precision, resolution, and known artifacts. Users of MLS data need to be familiar with information in the data quality document, and are encouraged – especially with this initial version of the data – to contact the MLS science team (e-mail [data@mls.jpl.nasa.gov](mailto:data@mls.jpl.nasa.gov)) on their usage and any problems or questions about the data. EOS MLS data, starting with v1.5, are available from the NASA Goddard Space Flight Center Earth Distributed Active Archive Center (DAAC) (<http://disc.gsfc.nasa.gov/Aura>).

Table XI gives examples of estimated precision for the MLS v1.5 data products. Absolute accuracy, to be determined as part of validation activities now underway, is expected to be typically 5-10% for composition and  $\sim 2$  K for temperature, and (like precision) will vary with the specific measurement and altitude. Some early validation analyses are in [62].

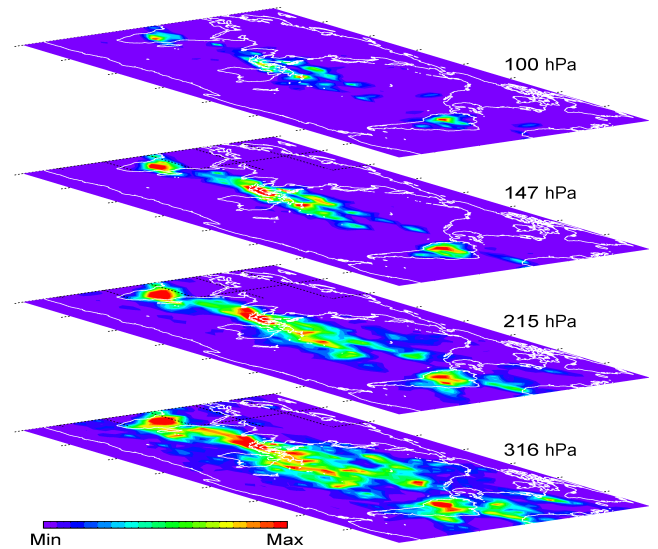


Fig. 18. EOS MLS measurements of cloud ice. Maps shown here give average values for December 2004 at four pressure levels. The color bar gives the average ice density ( $\text{mg}/\text{m}^3$ ) over the extent of the MLS field-of-view: min value for each layer is 0; max value is 1.2 for 100 hPa, 4.5 for 147 hPa, and 9 for 215 and 316 hPa.

TABLE XI  
Vertical range of usefulness and representative examples of estimated precision and vertical resolution for the MLS v1.5 data products.

data product (alphabetical order)	atmospheric pressure range of usefulness (hPa)	Estimated single profile precision (corresponding vertical resolution)	Estimated monthly zonal mean precision, for 5° zonal means unless otherwise noted (corresponding vertical resolution)
BrO	10 – 2.2	0.2-0.5 ppbv [not useful]; depending on height; averaging $n$ profiles improves by factor of $\sqrt{n}$	5-10 pptv ( $\sim 3$ km) for 30° latitude bins
ClO	100 – 1	0.1-0.2 ppbv (3-5 km)	5-10 pptv (3-5 km)
<sup>a</sup> CO	215 – 0.0046	0.01-0.02 ppmv ( $\sim 4$ km) @ 215-10 hPa $\sim 0.1$ ppmv ( $\sim 4$ km) @ 1 hPa $\sim 4$ ppmv ( $\sim 6$ km) @ 0.01 hPa	to be determined @ 215-10 hPa $\sim 4$ ppbv ( $\sim 4$ km) @ 1 hPa $\sim 0.2$ ppmv ( $\sim 6$ km) @ 0.01 hPa
geopotential height	316 – 0.001	$\sim 20$ m @ 100 hPa	to be determined
<sup>a,b</sup> H <sub>2</sub> O	316 – 0.1	$\sim 15\%$ (2-3 km) @ 316 hPa-tropopause $\sim 0.1$ ppmv (4-6 km) @ tropopause-1 hPa $\sim 0.3$ ppmv ( $\sim 8$ km) @ 0.1 hPa	$\sim 1\%$ (3-6 km) @ 316 – 1 hPa $\sim 1\%$ ( $\sim 8$ km) @ 0.1 hPa
<sup>a</sup> HCl	100 – 0.22	0.1-0.2 ppbv ( $\sim 3$ km) @ 100-10 hPa 0.2-0.3 ppbv (3-6 km) @ 10-0.2 hPa	5-10 pptv ( $\sim 3$ km) @ 100-10 hPa 10-20 pptv (3-6 km) @ 10-0.2 hPa
HCN	10 – 1.4	$\sim 50$ pptv ( $\sim 6$ km)	to be determined
<sup>a</sup> HNO <sub>3</sub>	147 – 3.2	$\sim 1$ ppbv (3-4 km)	to be determined
<sup>c</sup> HO <sub>2</sub>	22 – 0.22	0.3-2 ppbv [not useful]; depending on height; averaging $n$ profiles improves by factor of $\sqrt{n}$	$\sim 3$ pptv ( $\sim 3$ km) @ 22 hPa $\sim 20$ pptv ( $\sim 3$ km) @ 3 hPa for 30° latitude bins
HOCl	22 – 2.2	$\sim 5$ pptv ( $\sim 6$ km) @ 22-2.2 hPa	to be determined
ice water content	215 – 68	$\sim 4$ $\text{mg}/\text{m}^3$ ( $\sim 3$ km) @ 215 hPa $\sim 0.4$ $\text{mg}/\text{m}^3$ ( $\sim 3$ km) @ 100-68 hPa	to be determined
<sup>a</sup> N <sub>2</sub> O	100 – 0.1	10-20 ppbv (3-4 km) @ 100-1 hPa	to be determined
<sup>a</sup> O <sub>3</sub>	215 – 0.46	20-50 ppbv (4 km) @ 215-22 hPa 0.1-0.2 ppmv ( $\sim 3$ km) @ $\sim 22$ -0.46 hPa	1-2 ppbv @ tropopause – 0.46 hPa to be determined @ 215 - tropopause
<sup>c</sup> OH	46 – 0.22	$\sim 5$ pptv ( $\sim 3$ km) @ 46-10 hPa $\sim 25$ pptv ( $\sim 3$ km) @ 0.22 hPa	$\sim 0.2$ pptv ( $\sim 3$ km) @ 46-10 hPa $\sim 1$ pptv ( $\sim 3$ km) @ 0.22 hPa
<sup>a,b</sup> temperature	316 – 0.001	0.5-1 K (4-8 km) @ 316 – 0.1 hPa	to be determined

Values for precision are  $1\sigma$ . Numbers in parentheses give the approximate vertical resolution for the indicated precision: ppmv is parts per million ( $10^6$ ) by volume, ppbv is parts per billion ( $10^9$ ), and pptv is parts per trillion ( $10^{12}$ ).

<sup>a</sup>See [62] for more information on the quality and early validation of these products.

<sup>b</sup>Future data versions are expected to have improved vertical resolution for temperature and upper tropospheric H<sub>2</sub>O.

<sup>c</sup>See [52] for early validation analyses for OH and HO<sub>2</sub>.

## ACKNOWLEDGMENT

We thank colleagues at JPL and the University of Edinburgh for their help throughout development of EOS MLS. We thank JPL management, especially C. Elachi, for strong support over many years. Also for their support, we thank many members, both former and present, of the NASA GSFC project and Headquarters program offices - especially S. G. Tilford, R. J. McNeal, M. A. Luce, M. R. Schoeberl, M. D. King, P. DeCola, M. J. Kurylo, G. Asrar, R. A. Pickering, H. K. Ramapriyan and P. Sabelhaus. We thank the Raytheon ITSS team, especially M. Echeverri and E. Green for development and operation of the MLS Science Investigator-led Data Processing System (SIPS), and A. Hanzel for support. We thank A. E. Dessler, R. Fu, H. A. Michelsen, P. W. Mote and D. W. Waugh for contributions to documents formulating the MLS science objectives (some of which are included in this paper). Thanks to Xuan Sabounchi for assistance in preparing the manuscript.

## REFERENCES

- [1] J. W. Waters, "Microwave Limb Sounding," in *Atmospheric Remote Sensing by Microwave Radiometry* (M. A. Janssen, ed.), chapter 8, New York: John Wiley, 1993.
- [2] F. T. Barath, *et al.*, "The Upper Atmosphere Research Satellite Microwave Limb Sounder Instrument," *J. Geophys. Res.*, vol. 98, pp. 10,751-10,762, 1993.
- [3] J. W. Waters, *et al.*, "The UARS and EOS Microwave Limb Sounder Experiments," *J. Atmos. Sci.*, vol. 56, pp. 194-218, 1999.
- [4] M. J. Molina and F. S. Rowland, "Stratospheric sink for chlorofluoromethanes: Chlorine atom catalyzed destruction of ozone," *Nature*, vol. 249, pp. 810-812, 1974.
- [5] J. C. Farman, B. G. Gardiner, and J. D. Shanklin, "Large losses of total ozone in Antarctica reveal seasonal ClO<sub>x</sub>/NO<sub>x</sub> interaction," *Nature*, vol. 315, pp. 207-210, 1985.
- [6] S. Solomon, "The mystery of the Antarctic ozone hole," *Rev. Geophys.*, vol. 26, pp. 131-148, 1988.
- [7] J. W. Waters, *et al.*, "Stratospheric ClO and ozone from the Microwave Limb Sounder on the Upper Atmosphere Research Satellite," *Nature*, vol. 362, pp. 597-602, 1993.
- [8] G. L. Manney, *et al.*, "Chemical depletion of ozone in the Arctic lower stratosphere during winter 1992-93," *Nature*, vol. 370, pp. 429-434, 1994.
- [9] W. G. Read, *et al.*, "Upper-tropospheric water vapor from UARS MLS," *Bull. Am. Meteorol. Soc.*, vol. 76, pp. 2381-2389, 1995.
- [10] W. G. Read, *et al.*, "UARS Microwave Limb Sounder Upper Tropospheric Humidity Measurement: Method and Validation," *J. Geophys. Res.*, vol. 106, pp. 32,207-32,258, 2001.
- [11] W. G. Read, D. L. Wu, J. W. Waters, and H. C. Pumphrey, "Dehydration in the Tropical Tropopause Layer: Implications from UARS MLS," *J. Geophys. Res.*, vol. 109, no. D6, D06110, doi:10.1029/2003JD004056, 2004.
- [12] D. L. Wu, W. G. Read, A. E. Dessler, S. C. Sherwood, and J. H. Jiang, "UARS/MLS Cloud Ice Measurements: Implications for H<sub>2</sub>O Transport near the Tropopause," *J. Atmos. Sci.*, vol. 62, pp. 518-530, 2005.
- [13] M. L. Santee, *et al.*, "Interhemispheric differences in polar stratospheric HNO<sub>3</sub>, H<sub>2</sub>O, ClO and O<sub>3</sub>," *Science*, vol. 267, pp. 849-852, 1995.
- [14] M. L. Santee, G. L. Manney, N. J. Livesey, and W. G. Read, "Three-dimensional structure and evolution of stratospheric HNO<sub>3</sub> based on UARS Microwave Limb Sounder measurements," *J. Geophys. Res.*, vol. 109, D15306, doi:10.1029/2004JD004578, 2004.
- [15] D. L. Wu and J. W. Waters, "Satellite observations of atmospheric variances: A possible indication of gravity waves," *Geophys. Res. Lett.*, vol. 23, pp. 3631-3634, 1996.
- [16] C. McLandress, M. J. Alexander, and D. L. Wu, "MLS observations of gravity waves in the stratosphere: A climatology and interpretation," *J. Geophys. Res.*, vol. 105, pp. 11,947-11,967, 2000.
- [17] M. R. Schoeberl, *et al.*, "Overview of the EOS Aura Mission," *IEEE Trans. Geosci. Remote Sensing*, this issue.
- [18] R. Beer, "TES on the Aura Mission: Scientific Objectives, Measurements and Analysis Overview," *IEEE Trans. Geosci. Remote Sensing*, this issue.
- [19] P. F. Levelt, *et al.*, "The Ozone Monitoring Instrument," *IEEE Trans. Geosci. Remote Sensing*, this issue.
- [20] R. F. Jarnot, R. E. Cofield, J. W. Waters, D. A. Flower, and G. E. Peckham, "Calibration of the Microwave Limb Sounder on the Upper Atmosphere Research Satellite," *J. Geophys. Res.*, vol. 101, pp. 9957-9982, 1996.
- [21] R. E. Cofield and P. C. Stek, "EOS Microwave Limb Sounder GHz optics design and field-of-view calibration," *IEEE Trans. Geosci. Remote Sensing*, this issue.
- [22] R. F. Jarnot, V. S. Perun, and M. J. Schwartz, "Radiometric and spectral performance and calibration of the GHz bands of EOS MLS," *IEEE Trans. Remote Sensing*, this issue.
- [23] H. M. Pickett, "Microwave Limb Sounder THz Module on Aura," *IEEE Trans. Geosci. Remote Sensing*, this issue.
- [24] H. M. Pickett, R. L. Poynter, and E. A. Cohen, "Submillimeter, Millimeter, and Microwave Spectral Line Catalog," *Technical Report 80-23*, Jet Propulsion Laboratory, Pasadena, California, 1992.
- [25] B. J. Drouin, "Temperature Dependent Pressure Induced Lineshape of the HCl J=1←0 Rotational Transition in Nitrogen and Oxygen," *J. Quant. Spectrosc. Radiat. Transfer*, vol. 83, issues 3-4, pp. 321-331, 2004.
- [26] B. J. Drouin, J. Fisher, and R. R. Gamache, "Temperature dependent pressure induced lineshape of O<sub>3</sub> rotational transitions in air," *J. Quant. Spectrosc. Radiat. Transfer*, vol. 83, issue 1, pp. 63-81, 2004.
- [27] J. J. Oh and E. A. Cohen, "Pressure broadening of ClO by N<sub>2</sub> and O<sub>2</sub> near 204 and 649 GHz and new frequency measurements between 632 and 725 GHz," *J. Quant. Spectrosc. Radiat. Transfer*, vol. 54, pp. 151-156, 1994.
- [28] World Meteorological Organization (WMO), "Scientific assessment of ozone depletion: 2002," Executive summary released by WMO/UNEP, *World Meteorological organization*, Geneva, Switzerland, 2002.
- [29] R. R. Conway, M. E. Summers, M. H. Stevens, J. G. Cardon, P. Preusse, and D. Offermann, "Satellite Observations of Upper Stratospheric and Mesospheric OH: The HO<sub>x</sub> Dilemma," *Geophys. Res. Lett.*, vol. 27, pp. 2613-2616, 2000.
- [30] K. H. Rosenlof, *et al.*, "Stratospheric water vapor increases over the past half-century," *Geophys. Res. Lett.*, vol. 28, pp. 1195-1198, 2001.
- [31] V. L. Dvortsov and S. Solomon, "Response of the stratospheric temperatures and ozone to past and future increases in stratospheric humidity," *J. Geophys. Res.*, vol. 106, pp. 7505-7514, 2001.
- [32] R. W. Spencer and W. D. Braswell, "How dry is the tropical free troposphere? Implication for global warming theory," *Bull. Amer. Meteor. Soc.*, vol. 78, pp. 1097-1106, 1997.
- [33] J. T. Houghton, *et al.*, eds., *Climate Change 2001: The Scientific Basis*, Intergovernmental Panel on Climate Change, Cambridge University Press, Cambridge, UK, 2001.
- [34] P. M. Forster and K. P. Shine, "Radiative forcing and temperature trends from stratospheric ozone changes," *J. Geophys. Res.*, vol. 102, pp. 10,841-10,855, 1997.
- [35] P. M. Forster and K. P. Shine, "Assessing the climate impact of trends in stratospheric water vapor," *Geophys. Res. Lett.*, vol. 29, no. 6, 10.1029/2001GL013909, 2002.
- [36] N. J. Livesey, M. D. Fromm, J. W. Waters, G. L. Manney, M. L. Santee, and W. G. Read, "Enhancements in lower stratospheric CH<sub>3</sub>CN observed by UARS MLS following boreal forest fires," *J. Geophys. Res.*, vol. 109, no. D6, D06308, doi:10.1029/2003JD004055, 2004.
- [37] P. H. Siegel, *et al.*, "Heterodyne radiometer development for the Earth Observing System Microwave Limb Sounder," in *Infrared and Millimeter-Wave Engineering, SPIE 1874*, p. 124, 1993.
- [38] S. Weinreb, P. C. Chao, and W. Copp, "Full Waveguide Band, 90 to 140 GHz MMIC Amplifier Module," *1997 IEEE MTT-S Digest*, pp. 1279-1280, 1997.
- [39] M. C. Gaidis, H. M. Pickett, C. D. Smith, S. C. Martin, R. P. Smith, and P. H. Siegel, "A 2.5-THz Receiver Front End for Spaceborne Applications," *IEEE Trans. Microwave Theory Tech.*, vol. 48, pp. 733-739, 2000.

- [40] R. LaBelle, "A Channelized 2<sup>nd</sup> IF/LO Downconverter for the EOS Microwave Limb Sounder," in *Proc. 33<sup>rd</sup> European Microwave Conference*, Munich, 2003, pp. 1143-1146.
- [41] W. G. Read, Z. Shippony, M. J. Schwartz, N. J. Livesey, and W. V. Snyder, "The clear-sky unpolarized forward model for the EOS Aura Microwave Limb Sounder (MLS)," *IEEE Trans. Geosci. Remote Sensing*, this issue.
- [42] N. J. Livesey, W. V. Snyder, W. G. Read, and P. A. Wagner, "Retrieval algorithms for the EOS Microwave Limb Sounder," *IEEE Trans. Geosci. Remote Sensing*, this issue.
- [43] D. T. Cuddy, M. D. Echeverri, P. A. Wagner, A. T. Hanzel, and R. A. Fuller, "EOS MLS Science Data Processing System: A Description of Architecture and Capabilities," *IEEE Trans. Geosci. Remote Sensing*, this issue.
- [44] N. J. Livesey and W. G. Read, "Direct Retrieval of Line-of-Sight Atmospheric Structure from Limb Sounding Observations," *Geophys. Res. Lett.*, vol. 27, pp. 891-894, 2000.
- [45] M. J. Schwartz, W. G. Read, and W. V. Snyder, "Polarized radiative transfer for Zeeman-split oxygen lines in the EOS MLS forward model," *IEEE Trans. Geosci. Remote Sensing*, this issue.
- [46] D. L. Wu, J. H. Jiang, and C. P. Davis, "EOS MLS Cloud Ice Measurements and Cloudy-Sky Radiative Transfer Model," *IEEE Trans. Geosci. Remote Sensing*, this issue.
- [47] N. J. Livesey, *et al.*, "EOS MLS Version 1.5 Level 2 data quality and description document," JPL Technical Document D-32381, available at <http://mils.jpl.nasa.gov>, 2005.
- [48] Y. Jiang, "EOS MLS Level 3 Algorithm Theoretical Basis," JPL document D-18911, available at <http://mils.jpl.nasa.gov>, 2005.
- [49] M. L. Salby, "Sampling theory for synoptic satellite observations. Part II. Fast Fourier mapping," *J. Atmos. Sci.*, vol. 39, pp. 2601-2614, 1982.
- [50] M. L. Santee, *et al.*, "Polar processing and development of the 2004 Antarctic ozone hole: First results from Aura MLS," *Geophys. Res. Lett.*, vol. 32, L12817, doi:10.1029/2005GL022582, 2005.
- [51] G. L. Manney, *et al.*, "EOS Microwave Limb Sounder observations of the Antarctic polar vortex breakup in 2004," *Geophys. Res. Lett.*, vol. 32, L12811, doi:10.1029/2005GL022823, 2005.
- [52] H. M. Pickett, *et al.*, "Validation of Aura MLS HO<sub>x</sub> measurements with remote-sensing balloon instruments," *Geophys. Res. Lett.*, to be published.
- [53] H. M. Pickett, unpublished.
- [54] M. J. Filipiak, *et al.*, "Carbon monoxide measured by EOS MLS on Aura: First results," *Geophys. Res. Lett.*, vol. 32, L14825, doi:10.1029/2005GL022765, 2005.
- [55] Q. B. Li, *et al.*, "Convective outflow of South Asian pollution: A global CTM simulation compared with Aura MLS observations," *Geophys. Res. Lett.*, vol. 32, L14826, doi:10.1029/2005GL022762, 2005.
- [56] J. -L. Li, *et al.*, "Comparison of EOS MLS cloud ice measurements with ECMWF analyses and GCM simulations: Initial results," *Geophys. Res. Lett.*, vol. 32, L18710, doi:10.1029/2005GL023788, 2005.
- [57] C. P. Davis, D. L. Wu, C. Emde, J. H. Jiang, R. E. Cofield, and R. S. Harwood, "Cirrus induced polarization in 122 GHz Aura MLS radiances," *Geophys. Res. Lett.*, vol. 32, L14806, doi:10.1029/2005GL022681, 2005.
- [58] D. L. Wu, unpublished.
- [59] W. G. Read, unpublished.
- [60] D. L. Wu, unpublished.
- [61] V. Limpasuvan, D. L. Wu, M. J. Schwartz, J. W. Waters, Q. Wu, and T. L. Killeen, "The two-day wave in EOS MLS temperature and wind measurements during 2004-2005 winter," *Geophys. Res. Lett.*, vol. 32, L17809, doi:10.1029/2005GL023396, 2005.
- [62] L. Froidevaux, *et al.*, "Early Validation Analyses of Atmospheric Profiles from EOS MLS on the Aura Satellite," *IEEE Trans. Geosci. Remote Sensing*, this issue.



**Joe William Waters** was born 12 January 1944 on a farm in Montgomery County, Tennessee. He received B.S. and M.S. degrees in 1967, and Ph.D. in 1971, all from the Department of Electrical Engineering, Massachusetts Institute of Technology. His Ph. D. topic, supervised by D.H. Staelin, was on microwave remote sensing of the stratosphere.

He was on the research staff of the MIT Research Laboratory of Electronics from 1971 until 1973, and responsible for retrievals of atmospheric temperature profiles from the Nimbus-5 Microwave Spectrometer. Since 1973 he has been with the Jet Propulsion Laboratory, Pasadena, California. In 1974 Dr. Waters started development of the microwave limb sounding technique and the MLS experiments, which he has led since then. These progressed through experiments on aircraft, balloon, the Upper Atmosphere Research Satellite, and – as described in this paper – on the Earth Observing System Aura satellite. He is currently a Senior Research Scientist at JPL, and heads research groups in the JPL Science Division and the Instrument and Science Data Systems Division. Dr. Waters is the author of more than 150 peer-reviewed publications. He has twice been awarded the NASA Exceptional Scientific Achievement Medal.